Contributions to the FEL'98 Conference, August 17-21, 1998 in Williamsburg, USA

Contents

Influence of Electron Beam Halos on the FEL performance

B. Faatz and S. Reiche

Deutsches Elektronen-Synchrotron DESY, Notkestraße 85, 22603 Hamburg, Germany

Abstract

For single-pass free electron lasers (FEL), such as amplifiers and SASE device, saturation of the radiation power has to be reached within the length of the undulator. Therefore, detailed knowledge of electron beam parameters is crucial. So far, simulations have been performed with a given rms emittance and energy spread. At short radiation wavelengths, bunch compressors are used to compress the electron beam to achieve the desired high peak currents. In addition, external focusing along the entire undulator is used to maintain a constant small radius. The rotation of phase space due to compression might lead to a significant part of the bunch in tails that could increase the gain length. Furthermore, it is in general not possible to match both the beam core and the tail to the focusing structure. In this contribution, the influence of these tails, both transverse and in energy, on the FEL performance will be investigated. Simulations will be performed for beam parameters that have been assumed for the TESLA Test Facility (TTF) FEL at DESY.

1. Introduction

In many existing Free Electron Lasers, radiation power is amplified using a feedback system. In such a system, the most crucial constrain is that the gain exceeds the sum of all losses. As long as the number of passes needed to reach saturation is small compared to the total number of roundtrips of the field inside the cavity, the exact value of the single pass gain is of less importance. For a single pass device, more detailed knowledge of all parameters reducing the gain has to be obtained in order to determine the undulator length. In most studies thus far, the influence of beam emittance and energy spread has been investigated. In addition, a more exact estimate of the shotnoise power (in case of a SASE FEL [2]), the influence of magnetic errors and any misalignment [3] has been studied by several authors. In all these studies, however, the electron beam was assumed to be either Gaussian or parabolic. This is not neccesarily the case. First simulation studies of the bunch compressor of the TESLA Test Facility [1] have shown that the electron beam can have either tails or spatially separated distributions, both in any transverse plane and in energy. In this paper, the influence of two possible distributions on the FEL performance is studied. Two identical Gaussian distributions, spatially separated in the x-direction, are used. Only their distance and relative fraction is varied. Independently, two Gaussian distributions with the same central energy, but with different rms-width provide the initial settings for the studies. The fraction of the two distribution has been change in the same manner as for the transverse displacement.

2. Results

Table 1. Undulator and optics parameters for the TTF FEL (Phase I at 230 MeV).

Electron beam	
Peak current	500 A
Normalized rms emittance	2π mmmrad
rms energy spread	500 keV
average beam size	77 μm
ρ-parameter	$4 \cdot 10^{-3}$
undulator	
period length	27.3 mm
undulator peak field	0.497 T

Simulations with GENESIS 1.3 [4] have been performed for the TTF-FEL parameters. This is a fully 3 dimensional code, including time dependence. For these simulations, only the time-independent part has been used. Deviating from the TTF parameters the FODO-structure has been changed to get an almost constant β-function, with the average value equal to the value resulting from the real structure.

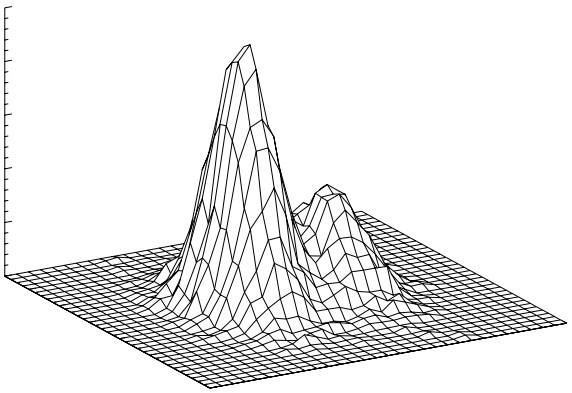

Fig. 1. *Example of a transverse electron beam distribution, in this case separated by 250 μm. The smaller Gaussian contains 30% of the charge.*

A first set of simulations has been performed assuming two identical Gaussian distributions, spatially separated by a certain amount in the x-direction. An example, with an offset of 250 μm and a charge of 70% in the large Gaussian and 30% in the smaller, is shown in Fig. 1. A similar displacement in y, or an initial kick in either x or y-direction would give similar results, the latter due to the FODO-structure, which makes the electron beam perform a betatron oscillation.

Results are shown in Fig. 2. The displacement in x varies from 50 to 250 μm, with the center of the total beam always on axis, e.g. $< x >= 0$. This means that, depending on the fraction in both distributions and on their relative offset, both are off-axis, performing a betatron oscillation. The rative fraction of the smaller Gaussian increases from 10% to 50% if saturation is reached within 17.5m. Especially for larger offsets saturation is only reached for smaller fractions. The normalized emittance given in the horizontal scale is calculated in the usual way, e.g. $e_x^2 =< \Delta x^2 >< \Delta x'^2 > - < (\Delta x \Delta x')^2 >$. As it can be seen, independent of the offset of the beams or their relative fraction, both power and saturation length seem to be related to the emittance calculated this way. One can also calculate the saturation power and length for an electron beam without halo, but with the same normalized emittance and the same mismatch of the initial conditions (resulting in the same beam envelope along the longitudinal axis). The results are within a few percent of the results shown in Fig. 2.

More important is, however, whether it is benificial to cut away part of the electron beam, place the remainder on axis and match it to the FODO-lattice. Resuts are shown to the right in Fig. 2. The reduction in current varies from 10% to 30%. As can be seen, within the parameter range studied, the saturation length for a given fraction in the halo tends towards the point where the current has been reduced

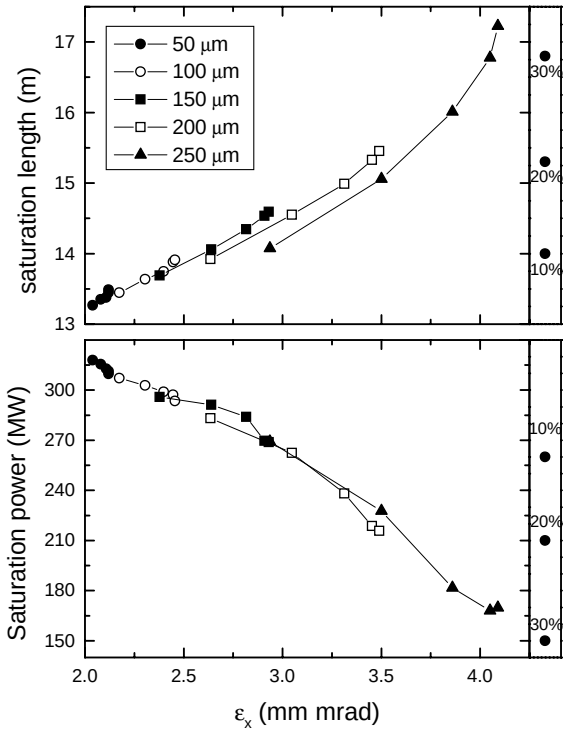

Fig. 2. *Saturation length (top figure) and power (bottom figure) versus normalized emittance for an electron beam consisting of two Gaussians separated in the x-direction in the range 50–250 μm. The fraction of electrons in one distribution varies from 10% to 50%, keeping the total charge constant. The points on the right indicate the saturaion length and power for a single Gaussian beam with a reduced current given by the indicated fraction.*

by the same amount. If one would not place the center of the beam on axis, but the largest fraction of the beam (90 to 50%), reducing the current gives similar results.

For a fraction of 20% in the halo, the offset has been extended to 500 μm. Results are shown in Fig. 3. In this case, two different positions of the beam are studied. In the top figure, the largest fraction of the beam is put on axis. For smaller offsets, this gives a slightly larger saturation length because of the large betatron oscillation performed by the off-axis part. For very large offsets, however, the 20% fraction no longer participates in the interaction and the saturation length and power are equal to the values obtained by cutting away this part of the current. In the bottom figure, the saturation length is slightly shorter for small offsets. As the offset increases, the saturation length increases beyond the value obtained for a 20% reduced current, because the large betatron oscillation of both parts of the beam reduce the interaction with the field. Therefore, the saturation length still increases (and the power decreases), but at a smaller rate than before.

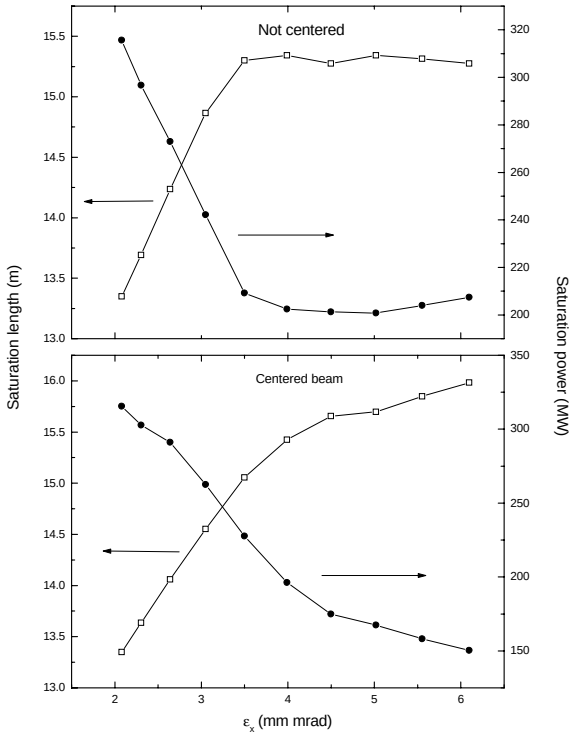

Fig. 3. *Saturation length versus normalized emittance for an electron beam consisting of two Gaussians separated in the x-direction in the range 50–500 μm. The fraction of electrons in one distribution is 20%. Either the largest fraction is put on axis (top figure) or the center of the entire beam, as before (bottom figure).*

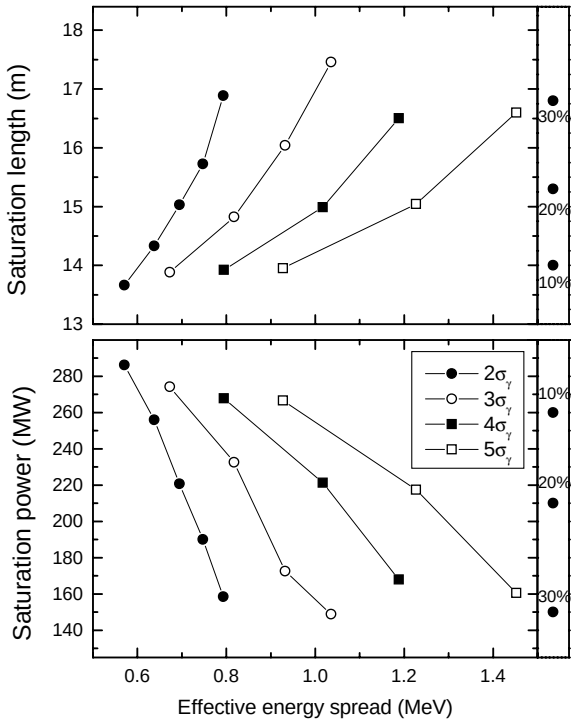

Fig. 4. *Saturation length (top figure) and power (bottom figure) versus effective energy spread for an electron beam consisting of two Gaussians in energy. The core beam always has the same energy width, the halo has a width of up to 5 times the width of the core beam. The fraction in the two parts varies from 10% and 90% to 50% in both. The points on the right indicate the saturaion length and power for a single Gaussian beam with a reduced current given by the indicated fraction.*

The next set of simulations shows the influence of two overlapping Gaussians in energy. Fig. 4 shows saturation power and length for an energy width of the halo compared to the core of the beam from 2 to 5 times. In case the halo has a two times larger energy width up to 50% halo, saturation is still reached within the undulator length studied here. For a larger width this number decreases to 30%. The horizontal scale, the effective energy spread (given in MeV), is simply $< \gamma^2 > - < \gamma >^2$, with γ the Lorentz factor. There is no obvious relation between this parameter and the gain. Simulations of a single Gaussian energy distribution with this same width give different results. As can be seen, the levels are almost constant for an energy spread of the halo exceeding $2\sigma_\gamma$. In turn, these values are almost identical to the results with the current reduced by the same fraction as it was in the halo. This can be understood as follows. The energy spread of the normal beam without halo is about half of the ρ-parameter. The bucket in longitudinal phase space in which the electrons are captured have a height of no more than ρ, a value which is reached close to saturation. All electrons outside of this region will not interact with the electron beam. Therefore, for a given fraction in the halo, increasing the energy spread will not change saturation power or length if it exceeds ρ significantly. Changing the fraction will, however, reduce the gain, because of a reduced part that remains captured inside the bucket.

3. Conclusions

Simulations of halos have shown that they can strongly influence the performance of the FEL. For transverse distribution consisting of two (partly) separated but otherwise equal distributions, one benefits from realigning the electron beam to get the center on axis and to minimize the betatron oscillations for small offsets. For larger offsets, the large betatron oscillation reduces the gain if the center is placed on axis. For two overlapping Gaussians in energy, both with the same central energy but with different width, the saturation length and power cannot be changed significantly. Cutting away the halo, if this would be possible, and this reducing the current, does not give a better preformance for the parameters studied here.

Acknowledgement

The authors would like to thank H.-D. Nuhn, C. Pagani and E.A. Schneidmiller for their usefull suggestions.

References

[1] DESY Print TESLA-FEL 95-03, Hamburg, DESY, 1995

[2] K.J. Kim, Nuc. Inst. & Meth., **A250** (1986) 396

[3] B. Faatz et al., Proceeding of the FEL 96 conference, (1997) 277

[4] S. Reiche, *GENESIS 1.3 - A Fully 3D Time Dependent FEL Simulation Code*, presented at this conference.

Regenerative FEL Amplifier at the TESLA Test Facility at DESY

B. Faatz[a], J. Feldhaus[a], J. Krzywinski[b],
E.L. Saldin[c], E.A. Schneidmiller[c], M.V. Yurkov[d]

[a] *Hamburger Synchrotronstrahlungslabor*

at Deutsches Elektronen-Synchrotron (DESY), Notkestrasse 85, D-22607 Hamburg, Germany

[b] *Institute of Physics of the Polish Academy of Sciences, 02688 Warszawa, Poland*

[c] *Automatic Systems Corporation, 443050 Samara, Russia*

[d] *Joint Institute for Nuclear Research, Dubna, 141980 Moscow Region, Russia*

Abstract

This paper presents a conceptual design of a regenerative FEL amplifier (RAFEL) as an extension of the single-pass free electron laser project at the TESLA Test Facility (TTF) at DESY. The proposed scheme requires the additional installation of only two optical components for a narrow-band feedback system and is fully compatible with the present design and the infrastructure developed for the TTF FEL project. It would allow to construct a tunable VUV laser with a minimum wavelength around 60 nm, a pulse duration of about 1 ps, a peak power of about 300 MW and an average power of about 25 W. The output radiation of the regenerative FEL amplifier would possess all the features which are usually associated with laser radiation: full transverse and longitudinal coherence and shot-to-shot stability of the output power. The degeneracy parameter of the output radiation would be about 10^{14} and thus have the same order of magnitude as that of a quantum laser operating in the visible.

1. Introduction

Free-electron laser techniques provide the possibility to extend the energy range of lasers into the vacuum ultraviolet (VUV) and X-ray regime using a single-pass free electron laser (FEL) amplifier based on the self-amplification of spontaneous emission (SASE). A characteristic feature of a single-pass SASE FEL is its rather large amplification bandwidth. When the process of amplification starts from noise, it produces a relatively wide spectrum of output radiation with only a short length of longitudinal coherence. The relative bandwidth at VUV wavelengths would be of the order of one per cent. Each radiation pulse consists of many independent wavepackets. The length of each wavepacket is much less than the radiation pulse length and there is no phase correlation between them.

For many applications this behavior is a serious limitation because, for example, one would observe large intensity fluctuations behind a narrow-band monochromator. Therefore, the improvement of the longitudinal coherence of VUV and X-ray FELs is of great practical importance. In order to obtain full longitudinal coherence it is necessary to seed the FEL amplifier with a sufficiently narrow band of radiation at a power level well above the effective power of shot noise in the electron beam. The optimum bandwidth of the seeding radiation, $\Delta\lambda/\lambda$, is related to the pulse length σ_z by $\Delta\lambda/\lambda = \lambda/\pi\sigma_z$. In this paper we present the seeding scheme based on the concept of Regenerative FEL amplifier (RAFEL) [1] which will be incorporated into the FEL project at the TESLA Test Facility (TTF) at DESY [2].

2. Properties of the TTF FEL without seeding

The RAFEL will be installed at the end of the first stage (Phase I) of the TTF FEL project . During this phase the linear accelerator will operate at electron beam energies up to 390 MeV and the FEL will

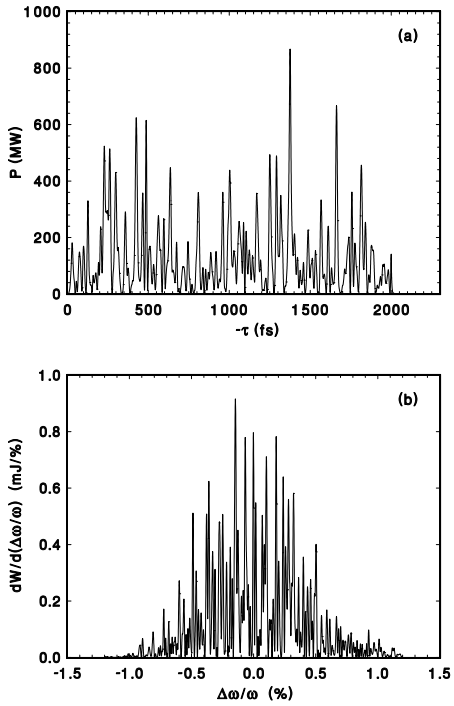

Fig. 1. Typical temporal structure (a) and spectrum of the radiation pulse (b) at the exit of 70 nm SASE FEL.

Table 1. Parameters of the RAFEL at the TESLA Test Facility

Parameters of the electron beam	
Energy	180-325 MeV
Charge per bunch	1 nC
Peak current	500 A
Bunch length (RMS)	250 μm
Bunch width (RMS)	70 μm
Energy spread (RMS)	500 keV
Normalized emittance (RMS)	2 mm mrad
Number of bunches per train	7200
Bunch separation	111 ns
Repetition rate	10 Hz
Parameters of the planar undulator	
Period	2.73 cm
Magnetic gap	12 mm
Peak magnetic field	0.497 T
Length of undulator module	4.5 m
Number of modules	3
Parameters of the feedback system	
Distance between mirrors	66.4 m
Monochromator resolution	5×10^{-5}
Total transmission	5×10^{-4}
Parameters of the radiation	
Wavelength	60-200 nm
Micropulse duration (RMS)	500 fs
Energy in the radiation pulse	0.36 mJ
Peak output power	300 MW
Average power	25 W

produce radiation with a wavelength down to ∼40 nm. Phase I is intended to test various novel hardware components and to prove the SASE principle for the first time at short wavelengths. In Phase II of the project the accelerator will be extended to increase the electron beam energy to more than 1 GeV and to drive a FEL facility down to wavelengths of a few nanometers.

The radiation from a high-gain SASE FEL is spatially (or transversely) coherent. The temporal (or longitudinal) coherence, however, is poor due to the start-up from noise. Consequently, also the frequency spectrum exhibits a similar structure (Fig. 1). It is interesting to note that the characteristic line width in the frequency domain which is determined by the bunch length, is close to the natural linewidth of atomic core levels given by the lifetime of the excited states. If one would select such a narrow band of radiation by a monochromator behind the FEL, the output intensity would change from pulse to pulse with a probability distribution close to the negative exponential distribution with the normalized standard deviation equal to 1 [3]. On the other hand, if seeding were possible, the spectral brilliance would be much higher and intensity fluctuations could be reduced to small level even for the smallest possible bandwidth given by the bunch length, providing ideal conditions for high resolution spectroscopy.

3. Regenerative FEL amplifier at the TTF

The technical parameters of the VUV FEL at DESY are such that it can be easily extended by a narrow-band optical feedback system turning the single-pass SASE FEL starting from noise into a regenerative FEL amplifier [4] which could provide fully coherent, powerful VUV laser radiation continuously tunable between approximately 200 nm and 60 nm. The optical system consists of only a mirror and a grating, because one can use optical components with good reflectivity near normal incidence. SiC appears to be particularly well suited for the energy range of the Phase I facility (see Fig. 2). In addition, the installation of the feedback is greatly facilitated by the fact that there is free space available for the optical components at exactly twice the distance between two electron bunches when the accelerator is operated in a 9 MHz multi-bunch mode. The schematic layout of the feedback system is shown in Figure 3.

The first bunch in a train of up to 7200 bunches amplifies shot noise and produces intense, but wide-band radiation as shown in Fig. 1. A fraction of the

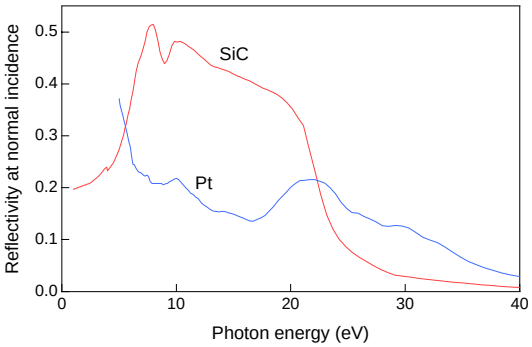

Fig. 2. Reflectivity of SiC and Pt at normal incidence calculated from the optical constants using REFLEC [5].

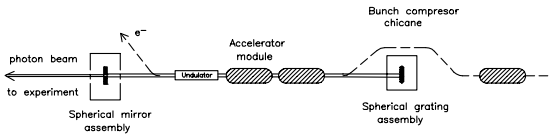

Fig. 3. Layout of Regenerative FEL amplifier at the TESLA Test Facility.

radiation is back-reflected by a spherical mirror using a magnification of the order of one. The spherical grating in Littrow mounting which is installed in a straight section in the electron bunch compression area between the first and the second accelerator module, disperses the light and focuses a narrow band of radiation back on the entrance of the undulator.

Calculations show that the aberrations in the optical system can be reduced down to the required level [4]. An alignment accuracy of about 2 μrad is sufficient for the reliable operation of the optical feedback. The alignment of the system can be made by conventional surveying techniques reducing the number and the values of free parameters to a minimum. This should allow to achieve the optimum overlap between photon and electron bunches within 10 to 20 steps in either direction of the grating.

The bandwidth of the feedback is chosen as to produce a photon pulse length about four times as long as the electron bunch length in order to avoid effects from a $\pm$ 1 ps time jitter. This requires a resolving power $\lambda/\Delta\lambda = 2 \cdot 10^4$ at $\lambda =$ 120 nm. If the distance between mirror and grating is properly adjusted, the monochromatic photon pulse coming from the first electron bunch in the train travels together with the fifth electron bunch. At the entrance of the undulator the overlap is optimum and the power density of the monochromatic light exceeds that of the shot noise by about three orders of magnitude such that it is amplified to saturation on its way through the undulator. Hence, the fifth and all following pulses exhibit the narrow bandwidth determined by the pulse length at a nearly constant, saturated power level with only little dependence on the input power of the seeding pulse. Accordingly, the time evolution of the light pulse will be smooth and the radiation will be fully coherent. Since the total saturated pulse energy is independent of the bandwidth of the seeding radiation provided it is smaller than the amplifier bandwidth, the spectral brilliance of the RAFEL is approximately two orders of magnitude larger than that of the SASE FEL.

The optical system shown in Figure 2 is only intended to test the seeding at short wavelengths and to gain experience with the FEL operating in the deep saturation regime. In order to minimize effort and risk, the optical system has been simplified as much as possible, particularly in order to facilitate the alignment and stability of the system at a distance of 66.4 m between mirror and grating. The characterization of the radiation will be done by measuring the intensity and the spectral distribution of the photons scattered from a thin probing wire in the beam.

If one wanted to use the output radiation for experiments, one would drill a central hole into the mirror M passing up to 90% of the radiation to the experiment. However, the hole in the mirror causes diffraction which dominates the propagation of the light and thus has to be taken into account in the design of the optical system. During a preliminary study [4] we have investigated a similar system with a plane mirror reflecting ~90% of the radiation to an experiment and passing the central part of the beam through a 1 mm hole to a spherical mirror. In this study the spherical grating was replaced by a plane grating in a combination with a spherical mirror in order to improve the optical performance of the system over a wider spectral range.

4. Present status

At present the conceptual design of the RAFEL project is finished and the technical design of the feedback system is under the way. The feedback system will be installed at the TTF site in 1999. We expect that the experiment will start in the beginning of the year 2000.

Acknowledgments

We wish to thank P. Gürtler, T. Limberg, G. Materlik, T. Möller, U.-K. Müller, C. Pagani, J. Pflüger, J. Roßbach, J.R. Schneider, S. Schreiber, B. Sonntag and H. Weise for useful discussions. We are grateful

to U. Hahn, J. Halik, A. Kabel and W. Sobala for technical support.

References

[1] J. Goldstein, D. Nguyen and R. Sheffield, Nucl. Instrum. and Methods **A393**(1997)137.

[2] "A VUV Free Electron Laser at the TESLA Test Facility: Conceptual Design Report", DESY Print TESLA-FEL 95-03, Hamburg, DESY, 1995.

[3] E.L. Saldin, E.A. Schneidmiller and M.V. Yurkov, Opt. Commun. **148**(1998)383.

[4] B. Faatz, J. Feldhaus, J. Krzywinski, E.L. Saldin, E.A. Schneidmiller and M.V. Yurkov, "Regenerative FEL Amplifier at the DESY TESLA Test Facility as a Fully Coherent VUV Laser", DESY Print TESLA-FEL 97-07, Hamburg, DESY, 1997.

[5] F. Schäfers and M. Krumrey, BESSY Technical Report TB 201/96, 1996.

An FEL Based High Intensity Gamma-Source at the TESLA Test Facility at DESY

C. Pagani[a], E.L. Saldin[b], E.A. Schneidmiller[b], M.V. Yurkov[c]

[a] *INFN Milano - LASA, Via Cervi, 201, 20090 Segrate (MI), Italy*

[b] *Automatic Systems Corporation, 443050 Samara, Russia*

[c] *Joint Institute for Nuclear Research, Dubna, 141980 Moscow Region, Russia*

Abstract

One of the possible extension of the FEL activity at DESY is connected with the installation of an additional FEL beamline providing tunable UV radiation with the peak and average power of 220 GW and 7 kW, respectively. This report presents the feasibility study of a high intensity, polarized, monochromatic gamma-source at the TESLA Test Facility. Gamma-quanta are produced in the process of Compton backscattering of the UV FEL radiation on a 1 GeV electrons of the TTF accelerator. The ultimate intensity of the gamma-source can reach the value up to 10^{12} gamma-quanta per second with the maximal energy of about 100 MeV. Energy resolution of the gamma-source can be reduced down to the value of about 0.2 %. Potential applications of the intensive gamma-source at the TESLA Test Facility are discussed, too.

1. Introduction

The Compton backscattering of laser light on high energy electrons is considered now as the most promising way to obtain high-intensity monochromatic gamma-rays [1]. Recently several investigations have been performed showing the possibility of constructing the gamma-sources with the energy of gamma-quanta of the order of tens and hundreds of MeV and the ultimate intensity $10^{10} - 10^{14} s^{-1}$ [2, 3]. These proposals suggest to use the scattering of the free-electron laser (FEL) radiation on the electron bunches in a storage ring.

In this paper we point at the possibility of constructing the high-intensity gamma-source at a high power linear accelerator. A 1 GeV superconducting linear accelerator being under construction at the TESLA Test Facility (TTF) at DESY will produce electron beam with high average and peak power, low energy spread and emittance. The main practical application of this accelerator is to use it for driving the soft X-ray free electron laser [4]. It is proposed also to construct a high power UV free electron laser at the TTF [5, 6]. The radiation from a low-power master oscillator will be amplified in the FEL amplifier with a tapered undulator providing peak and average output power up to 220 GW and 7 kW, respectively. The Compton backscattering of this radiation on the TTF electron beam allows one to reach the intensity of the gamma-quanta up to $10^{12}\mathrm{s}^{-1}$ with the maximal energy of about 100 MeV. This unique gamma-source could be used for investigations in nuclear physics as well as for testing the technical solutions of positron sources and gamma-gamma options of the future linear colliders.

2. High intensity gamma-source

Powerful UV FEL at the TTF [5, 6] can be used for construction of a high intensity, polarized, monochromatic gamma-source. The scheme of the gamma-source is presented in Fig. 1. Gamma-quanta are produced in the process of the Compton backscattering of the laser photons on incoming electrons. The process of the FEL interaction induces the energy spread in the electron bunch. If the laser radiation will be scattered on the bunches involved in the FEL process, this will result in decreasing of the energy resolution of the gamma-source. To avoid this harmful effect, master laser should operate at a half of the repetition

rate of the electron bunches. So, the laser radiation amplified by an electron bunch is focused on the next, unperturbed electron bunch.

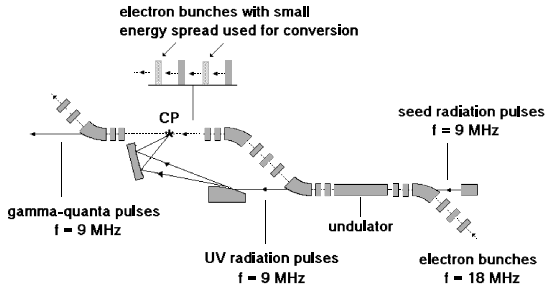

Fig. 1. Scheme of the gamma-source at the TESLA Test Facility.

The maximal energy of gamma-quanta is defined by the frequency of the primary photons ω and the energy of the electron $\mathcal{E}$: $(\hbar\omega_\gamma)_{\max} = \mathcal{E}\chi/(1+\chi)$. Here $\chi = 4\gamma\hbar\omega/m_e c^2$, m_e is the electron mass and $\gamma = \mathcal{E}/m_e c^2$ is relativistic factor. Maximal energy of gamma quanta is about 86 MeV at the wavelength of primary photon of 200 nm and the energy of electron of 1 GeV. In principle, the energy of the TTF accelerator can be upgraded up to the value of 2 GeV. In this case maximal available energy of gamma-quanta will be about 320 MeV. General parameters of the gamma-source at the TTF are presented in Table 1.

The frequencies of the incident and scattered photons, ω and ω_γ, are connected by the relation:

$$\hbar\omega_\gamma = \frac{\mathcal{E}\chi}{1+\chi+\gamma^2\theta^2} \ , \qquad (1)$$

where θ is the scattering angle. It is seen from eq. (1) that there is strict correlation between the energy of the backscattered photon and the scattering angle. This allows one to use angle selection technique for selecting the gamma-quanta with the required energy. In the case of monoenergetic and laminar electron beam this technique allows, in principle, to achieve any required energy resolution of gamma-quanta. In practice electron beam has finite energy spread which imposes a limit on minimal energy resolution of the gamma-source. Influence of the angle spread in the electron beam on the energy resolution of the gamma-source can be eliminated by an appropriate choice of the beta-function at the conversion point. The value of the rms angle spread in the electron beam is $\sigma_\theta = \sqrt{\epsilon/\beta}$, where ϵ is the emittance of the electron beam and β is beta-function at the conversion point. Minimal energy resolution of the gamma-source due to the angle spread is given by the expression:

$$(\Delta\hbar\omega_\gamma)/\hbar\omega_\gamma \simeq (\gamma\sigma_\theta)^2/2 \ . \qquad (2)$$

Table 1. Parameters of the gamma-source at the TESLA Test Facility

General parameters	
Maximal energy of gamma-quanta	85 MeV
Yield of gamma-quanta	10^{12}s^{-1}
Energy resolution	1 %
Angular divergence	0.5 mrad
Repetition rate	10 pps
Macropulse duration	800 μs
Number of pulses per macropulse	7200
Micropulse repetition rate	9 MHz
Micropulse duration (FWHM)	300 fs
Parameters of the electron beam	
Energy	1 GeV
Charge per bunch	1 nC
Energy spread (RMS)	1 MeV
Normalized emittance (RMS)	2 mm mrad
Beam size at the conversion point	14 μm
Bunch length (RMS)	50 μm
Parameters of the FEL	
Wavelength	208 nm
Micropulse duration	230 fs
Energy in the radiation pulse	50 mJ
Peak output power	220 GW
Average power	3.6 kW
Parameters of the focusing system	
Focuse distance of the mirror	3 m
Radiation spot size on the mirror	2.5 cm
Incident radiation flux on the mirror	350 W/cm^2
Reflectivity of the mirror	99 %
Radiation spot size	
at the conversion point	8 μm
Rayleigh length	1 mm
Conversion efficiency	0.23 %

It should be also noted that there is strict correlation between the energy of the gamma quantum and its polarization, so the angular selection provides not only monochromatization, but determines also the polarization of gamma quanta.

To obtain a higher yield of gamma-quanta one should provide maximal spatial density of the primary photons and of the electron beam in the conversion region. We assume the laser beam to be close to the Gaussian one. The power flux density in the waist of Gaussian laser beam is given by the expression $dP(r)/dS \propto \exp(-2r^2/w^2)$, where w is the size of the Gaussian beam waist. The Rayleigh length of the laser beam, $Z_R = \pi w^2/\lambda$, and the beta function of the electron beam focusing system, β, are assumed to be large with respect to the length of the laser and the electron pulse. Thus, we can neglect the change of the transverse size of the photon and electron pulses during the collision. As a result, the yield of gamma-quanta is [5]

$$\frac{dN_\gamma}{dt} = fN_e\delta\ , \qquad \delta = \frac{A\sigma_c}{2\pi\hbar\omega(\epsilon\beta + w^2/4)}\ , \qquad (3)$$

where A is the energy in the radiation pulse, f is the repetition rate of collisions, N_e is the number of electrons per bunch, δ is the conversion efficiency (number of gamma-quanta produced by one electron) and

$$\sigma_c = 2\pi r_e^2\left[\frac{1}{\chi}\ln(1+\chi) - \frac{8+4\chi}{\chi^3}\ln(1+\chi) + \frac{8}{\chi^2} + \frac{2+\chi}{2(1+\chi)^2}\right] \quad (4)$$

is the total Compton cross section on unpolarized electrons, where $r_e = e^2/m_ec^2$ is the classical radius of electron.

The ultimate energy resolution of the gamma-source presented in Fig. 1 is limited by the energy spread in the electron beam induced by the SASE FEL process. Even in the case when there is no seed signal at the entrance of the FEL amplifier, the process of the amplification of the radiation is triggered by the shot noise in the electron beam. Simulation of this process shows that the induced energy spread due to the SASE FEL process is about 5 MeV at the exit of the undulator [5] which imposes a limit on ultimate energy resolution of the gamma-source of 1 %. Taking into account the angular spread in the electron beam, beta function of the electron beam at the conversion point should be about 20 cm in order to provide this energy resolution. The radiation spot size at the conversion point has been set to $w \simeq 8$ μm (which corresponds to the Rayleigh length of 1 mm). In this case there are no fluctuations of the gamma-source intensity due to the time jitter of the electron pulse of about 1 ps. According to (3), at chosen parameters of the colliding photon and electron bunches conversion efficiency is about $\delta \simeq 0.23$ %. At the pulse repetition rate of the accelerator equal to 18 MHz the yield of gamma-quanta is about of 10^{12}s^{-1}.

There exists another option for organization of the conversion region prior the entrance of the electron beam into the undulator. It provides the possibility to double the yield of gamma-quanta, because each electron bunch can be used for producing gamma-quanta. Due to a small value of the conversion efficiency this will not destroy the electron beam and it can be used for the amplification of the radiation in the undulator. Besides, an ultimate energy resolution of the gamma-source of about 0.2 % can be achieved. This limit is defined by the energy spread in the electron beam of 1 MeV. The value of the beta function at the conversion point should be increased up to 1 m. The yield of the gamma-source with ultimate energy resolution of 0.2 % will be about of 2×10^{11}s^{-1}.

3. Possible applications for nuclear physics

The gamma-source at the TESLA Test Facility is a unique one providing an extremely high flux of polarized, monochromatic gamma-quanta. The proposed gamma facility is an extremely selective probe for investigations of not only conventional nuclear physics, but of exotic nuclear states (similar to those which occur inside the core of neutron stars or the quark-gluon plasma) and reaction mechanisms. Up to 200 MeV we are dealing with the internucleon distance about 1 fm (which is of the order of the size of nucleon). Nowadays the investigation of microscopic nuclear structure with resolution $\gtrsim$ 200 MeV is an unexplored field [7]. The idea is to work in the kinematical region where the processes on free nucleons are forbidden (the cumulative particle production or the underthreshold particle production). This intermediate energy region is covered by nonperturbative QCD effects. Investigations of this transition energy region, from the perturbative to nonperturbative QCD, are the most attractive direction for relativistic nuclear physics to understand the role of the nonnucleonic (pion, Δ, etc, and few-nucleon configurations) and quark-gluon degrees of freedom.

Another interesting topic of these investigations is a possibility to extract additional information about the hadron or the nuclear structure which is usually hidden in the spin-averaged analysis [8]. Polarization observables has a promise of opening a new field in the photoproduction of pion from nucleon and nuclear targets [9], in the processes of photodisintegration of the lightest nuclei [10, 11] and others. Many problems in photonucleon and photonulear physics are not resolved till now due to the lack of high quality photon beams.

4. Test facility for the positron source

The projects of the next generation linear colliders assume to produce positrons by gamma-quanta in a thin target [12, 13]. Gamma-quanta are produced by the spent electron beam in a long wiggler or undulator. For instance, in the TESLA project the 250 GeV electron beam passes a wiggler of 35 m length producing powerful gamma-beam [12]. The mean energy of gamma-quanta is about 25 MeV. Positrons produced in a thin target have large energy and angle spread. After the target they should be captured and accelerated. Such a complicated system requires experimental verification prior construction of the full-scale facility. The test facility can be constructed on the base of a high intensity gamma-source described above. Energy spectrum of the gamma-source is similar to that to be used in a full scale facility. Intensity of the gamma-source described above has been limited

by the requirement of the energy resolution. For the positron source test facility the value of the beta function at the conversion point can be reduced down to the value of about 1 cm (the angle divergence in the beam is about $1/\gamma$ in this case). As a result, the yield of gamma-quanta reaches the value of $10^{13}\mathrm{s}^{-1}$. Remembering that the conversion efficiency of gamma-quanta into electron-positron pair is about of 0.5 at the thickness of the target about one radiation length, we estimate the yield of the positrons to be about $5 \times 10^{12}\mathrm{s}^{-1}$. Such a positron yield is sufficient for operation of the test facility. Taking into account that TTF accelerator has the same time diagram of operation as TESLA accelerator, this facility will allow to verify experimentally all the systems of the positron source (optimization of the target, capture efficiency, etc).

The test facility for the positron source could reveal unique opportunity for experimental investigation of the polarized positron source proposed in ref. [14]. In this case FEL amplifier should be equipped with a helical undulator.

5. Test facility for the gamma-gamma collider

An option of a gamma-gamma collider is included in several projects of the future generation linear colliders [12, 13]. The scheme for organization of gamma-gamma collisions can be explained as follows. Two electron bunches are focused into the interaction point. Prior the collision each electron bunch is irradiated by a powerful laser pulse. High energy gamma-quanta are produced in the process of Compton backscattering and, following the electron trajectories, collide at the interaction region. The time structure of the laser pulses should be identical to the time structure of the electron bunches. It means, that the laser should have a capability of precise synchronization with the electron bunches and should provide a high repetition rate. The last parameter is extremely severe for the TESLA collider requiring a sub-terawatt level peak power laser with the repetition rate of about 1 MHz. In this case there is no reliable technical solution for a conventional laser system with required parameters, and free electron laser system is considered now as a candidate for the laser [12, 15]. Parameters of the high power UV FEL at the TTF and of the optical system of the gamma-source are very close to those used in the project of the gamma-gamma collider. Indeed, peak and average laser power of 220 GW and 7 kW, respectively, are close to those required for the gamma-collider. Time diagram of the laser pulses is similar to the time diagram of the TESLA collider. The problems connected with alignment of the mirrors, possible radiation damage of the mirrors, time jitters and the problems of focusing the laser beam in a tiny spot are similar to those to be met at a full-scale facility. So, successful realization of this project will serve as an experimental verification of a technical feasibility of the gamma-gamma option at TESLA.

References

[1] A. D'Angelo, "Review of Compton scattering projects", presented at the EPAC-98 Conference, Stockholm.

[2] E.L. Saldin et al., Nucl. Instrum. and Methods **A375**(1996)606.

[3] V. N. Litvinenko and J. M. J. Madey, Nucl. Instrum. and Methods **A375**(1996)580.

[4] J. Rossbach, Nucl. Instrum. and Methods **A375**(1996)269.

[5] C. Pagani, E.L. Saldin, E.A. Schneidmiller and M.V. Yurkov, " Design considerations and analysis of potential applications of a high power ultraviolet FEL at the TESLA Test Facility at DESY", DESY print, TESLA-FEL 98-03, Hamburg (1998).

[6] E.L. Saldin, E.A. Schneidmiller and M.V. Yurkov, "A high average power UV FEL at a 1 GeV superconducting linear accelerator at the TESLA Test Facility at DESY", presented at this Conference.

[7] L. Frankfurt, SLAC Workshop on High Energy Electroproduction and Spin Physics,
SLAC-392 Conf-920266 UC-414, 1992.

[8] R.P. Feynman, Photon-hadron interactions (W.A. Benjamin, Inc., 1972).

[9] A.A. Chumbalov et al.,Phys. Letters, B321(1994), 317-322; D. Drechsel, MKPH-T-93-9, Mainz, 1993.

[10] V. Isbert et al., DAPNIA/SPhN 93 64, C.E. Saclay, 1993

[11] H, Arenhövel and M. Sanzone, "Photodisintegration of the Deuteron", Springer-Verlag Wien – New York, 1991

[12] "Conceptual Design of a 500 GeV e+e− Linear Collider with Integrated X-ray Laser Facility" (Editors R.Brinkmann, G. Materlik, J. Rossbach, A. Wagner), DESY 97-048, Hamburg, 1997.

[13] "Zeroth-Order Design Report for the Next Linear Collider", LBNL-PUB-5424,SLAC Report 474, UCRL-ID-124161 (May 1996).

[14] V.E. Balakin and A.A. Mikhailichenko, Proc. of the 12th Int. Conference on High Energy Accelerators (Batavia, 1983), p. 127.
Preprint INP 79-85, Novosibirsk, 1979.

[15] E.L. Saldin et al., Nucl. Instrum. and Methods **A361**(1995)101.

Field fine tuning by pole height adjustment for the undulator of the TTF-FEL

J. Pflüger, H. Lu*, T. Teichmann

Hamburger Synchrotronstrahlungslabor HASYLAB
at Deutsches Elektronen-Synchrotron DESY
Notkestr85, 22603 Hamburg

**on leave from : FEL Laboratory at Institute for High Energy Physics (IHEP)*
P. O. Box 2732 Beijing 100080
P. R. China

Abstract

The field of the undulator for the VUV-FEL at the TESLA Test Facility has to meet very tough tolerances in order to guarantee a close overlap between the electron beam and the laser field. Consequently the undulator was designed to have height-adjustable poles in order to allow for fine tuning of the vertical undulator field in such a way that the trajectory is straightened. The signature of local pole height and gap changes on the field distribution was investigated. It was seen that changes are not restricted to the pole itself. Its effect can be seen up to the next eight neighboring poles.

In this contribution we describe an algorithm in detail, which allows the prediction of required pole height changes in order to correct for field errors. As input data field errors deduced from precise magnetic field measurements are used together with the signatures of pole movements. A band diagonal system of linear equations has to be solved to obtain the pole height corrections.

For demonstration of the method the field of the 0.9m long prototype structure was optimized to have a straight trajectory. Since only a sparse band diagonal system of equations has to be solved, the method has the potential to be used in very long undulators having 600 - 1000 poles.

Introduction

At DESY in Hamburg a Free Electron Laser (FEL) for the VUV spectral range down to 6.4nm using the principle of Self Amplified Spontaneous Emission (SASE) /1,2 / is under construction. It will use the electron beam generated by the TESLA Test Facility (TTF) /3,4/ and will be built in two stages which are described in detail in /3,5/. The complete undulator system has a maximum length of about 30m. It is a fixed gap structure and is described in detail in /6-9/. Table 1 reproduces its magnetic parameters. The device is a combined function undulator which integrates two functions: First it provides the sinusoidally shaped undulator field so that the FEL process can take place. Second an alternating gradient field of about ±20 T/m for the FODO lattice which is superimposed to the undulator field is generated.
The magnetic design was chosen to combine the following properties:

1. It is a completely planar structure, which allows for very good access to the field region at the beam position allowing for high accuracy field measurements as well as an easy installation of the vacuum chamber without breaking of any magnetic circuits.

2. The gradient can be as large as ≈20 T/m.
3. The exact value and the precise location of the quadrupole axis is fine tunable.
4. Undulator and focusing fields are decoupled. This means that on the quadrupole axis the sign and magnitude of the field gradient has no influence on the undulator field and vice versa.

Table 1: Undulator parameters for the undulator for the VUV - FEL at the TESLA Test Facility

Gap (fixed)	[mm]	12
Period Length	[mm]	27.3
Undulator Peak Field	[T]	0.5
K - Parameter		1.27
Design Gradient	[T/m]	18.3
Number of poles per undulator module		327
Total length per module	[mm]	4492.2
Length of FODO quad section	[mm]	136.5
FODO Period Length	[m]	0.9555
Number of FODO periods per module		5
Separation between undulator modules	[m]	0.2853

The magnetic fields of Undulators for SASE FELs have to meet tough specifications /10/. Careful optimization and fine tuning of an undulator is required after it has been assembled. Two steps are planned: First the "naked" undulator, i.e. the undulator without the focusing magnets will be measured and optimized in such a way as to obtain a straight trajectory in the horizontal and vertical plane. In the horizontal plane the height adjustable poles will be used to obtain an optimum B_y field distribution. In the vertical plane field errors are not expected to be serious. Good sorting of the magnets using simulated annealing will minimize residual error fields /11/in any case. Small remaining field errors can be treated using a very few suitable shims.
In a second step the focusing magnets will be attached and their strength as well as the exact position of quad centers will be fine tuned as described in ref. /12/.
This contribution deals with the tuning of the B_y field of the "naked" undulator. A numerical procedure which allows the prediction of pole adjustments to obtain a straight trajectory from precise magnetic measurements was developed and is described in detail.

Magnetic measurements, Experimental

The new 12m long bench was used to characterize the magnetic performance of the prototype structure. It provides sufficient mechanical accuracy for the magnetic measurements of the combined function undulator for the FEL at the TTF. Measurements could be performed with both high spatial and high field resolution. For the field measurements the resolution is given by $\Delta B/B \approx 5.10^{-4}$, the spatial resolution of the encoder system is 1 μm.
The magnetic measurements presented in this contribution were made on a 0.9m long prototype of the undulator for the VUV-FEL with the same parameters as in Table 1. The pole heights of this structure can be adjusted by tuning hex screws by an estimated ±0.5 mm. The screws having a 0.7mm pitch act on the poles under an angle of 60° so that there results a 3.9μm pole height change for a rotation angle of one degree on the tuning screws. The tuning screws were actuated manually using special hex keys with degree scales. Due to backlash between hex keys and the screws as well as to stick effects and elasticity in the 150mm long key it was estimated that the screws could be adjusted with an accuracy of about ± 5 to 10 degrees leading to a relative inaccuracy of the pole heights of about 20 - 40 μm.

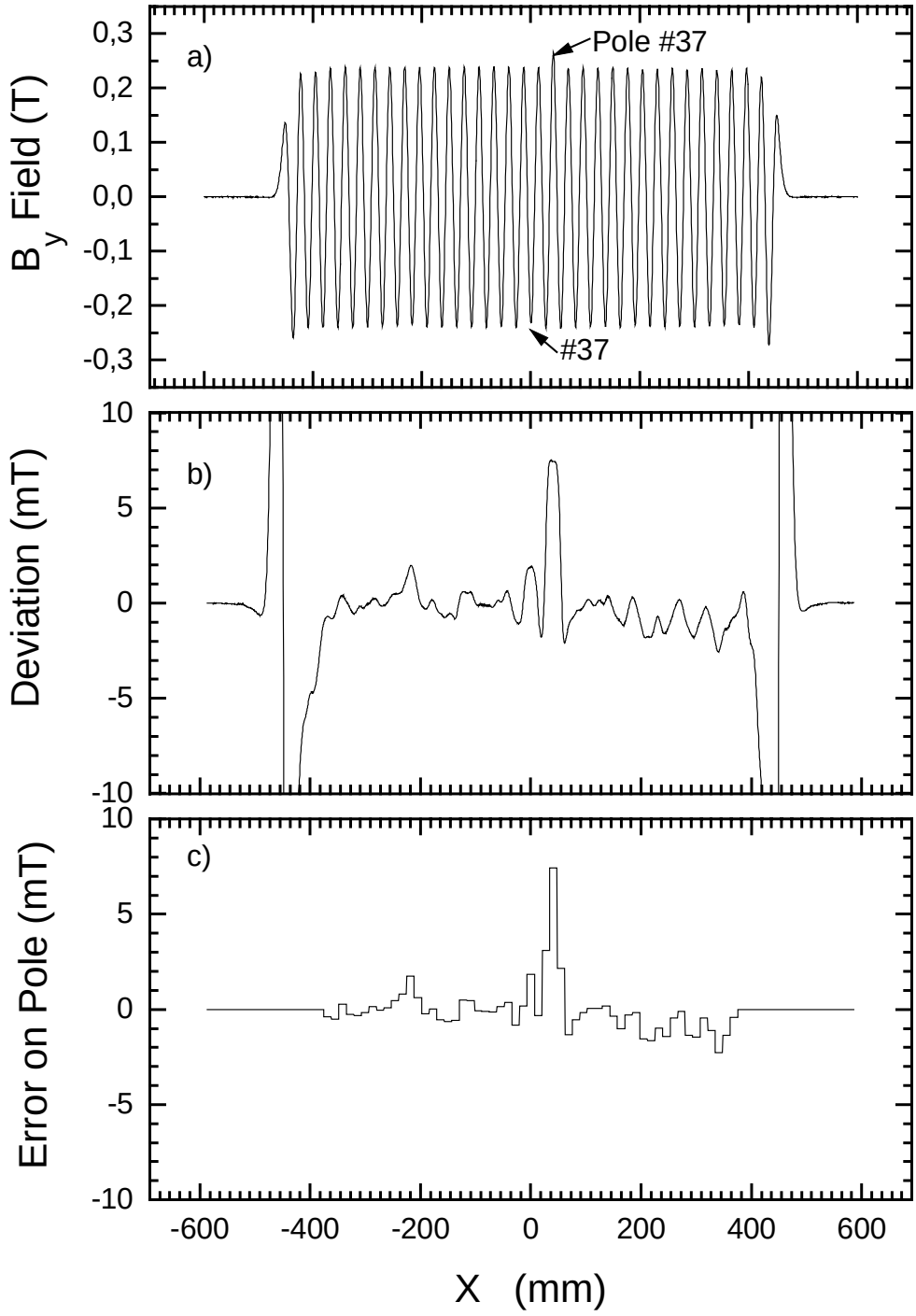

Fig 1 Example for generation of the errorfields on the poles for the upper structure half. The field was measured 6mm below the poles of the upper structure half at the nominal beam position at 12mm gap

a) Field data , Pole #37 has been detuned on purpose to demonstrate the effect

b) After application of the λ-filter. The large end excursion at the ends is an artefact of the λ-filter.

c) Average error field at the poles. Due to the convolution, the adjustment is now smeared out over next nearest neighbors. This is cleasly seen at Pole #37. The end region has been excluded

Description of the method

The idea for the error control by pole height adjustment is simple: Error fields are determined by means of precise magnetic measurements. Precise knowledge of the influence of pole height changes on the field distribution, the socalled signature can be obtained from magnetic measurements. Then an algorithm may be used to calculate the required pole shifts, which minimize these errors.
Similar approaches has been reported by Stoner and Bekefi /13/ who calculated shunt impedances to optimize the peak field homogeneity of a pulsed electromagnetic short period undulator and Ramian et. al /14,15 / who describe a robotic system which is able to fine tune the peak field of PM undulator systems. Due to the measurement techniques applied only the peak field was optimized in references /13-15/. In contrast the goal of this work was to optimize the comlete trajectory.
The treatment needs some assumptions and conventions, which are described below. In a first step the error field on each pole is determined by the "deviation" from the ideal field. Each pole is characterized by one number, the mean field deviation, which is the deviation averaged over the half period length of that pole at its nominal position. We tried two different ways to determine the deviation from the ideal field:

1. Applying a λ filter, which means convoluting the magnetic field data with a square function of width λ, the period length. In this way all the information with periodicity λ/n, $(n= 1,2,...)$ is removed from the data and only nonperiodic perturbations are left over. The convolution however smoothes the data and smears out spatial information over one period length.

2. Alternatively we tried various harmonic fits to the data up to order 11 to determine the periodic content and subtracted it from the field to obtain the deviation. This method gives noisier data, but preserves spatial information.

Both methods were compared and gave comparable results. Fig. 1 demonstrates the steps in the case of the application of a λ filter. Fig. 1a) shows the field distribution of the upper structure half of a 0.9m long prototype structure. One pole, #37, has been detuned on purpose to demonstrate how it shows up in the analysis. In Fig. 1b) the λ filter has been applied to the data of Fig. 1a). The perturbation applied on Pole #37 is now very clearly visible. The large excursion at the ends is an artefact of the λ filter. This region therefore has been excluded from the analysis. Fig. 1c) finally shows the assignment of field errors to the poles. The endpole region has been excluded. Spatial information is smeared out and the perturbation of pole #37 has now been split up on the next nearest neighboring poles as well. This is the input data to calculate the pole height adjustment.

In the second step we assume a linear relationship between the movement of a pole and the perturbation induced at any other pole. This is an assumption which only holds for small pole shifts of a few tenth of a millimeter. We assume an undulator consisting of N identical poles. Poles near the ends again have to be excluded, since due to the truncation they cannot be considered as identical with poles well inside the undulator. Excluding the outermost 4 to 5 poles was found to be sufficient to neglect both, artefacts from the λ filter and truncation effects as well.
We are interested in the field change S_j on a pole with index j if another pole with index i is moved by an amount p_i. In order to get the total field change on pole j one has to sum over all contributions from poles i .The S_j may be interpreted as minus the field change on pole j which is required to obtain a perfect undulator field.
These considerations lead to the following linear system of equations:

$$
\begin{array}{lcccccccccc}
S_1 & = & a_0 \cdot p_1 & + & a_1 \cdot p_2 & + & a_2 \cdot p_3 & +\ldots+ & a_{i-1} \cdot p_i & +\ldots+ & a_{N-1} \cdot p_N \\
S_2 & = & a_{-1} \cdot p_1 & + & a_0 \cdot p_2 & + & a_1 \cdot p_3 & +\ldots+ & a_{i-2} \cdot p_i & +\ldots+ & a_{N-2} \cdot p_N \\
S_3 & = & a_{-2} \cdot p_1 & + & a_{-1} \cdot p_2 & + & a_0 \cdot p_3 & +\ldots+ & a_{i-3} \cdot p_i & +\ldots+ & a_{N-3} \cdot p_N \\
\cdot & = & & & & & \cdot & & & & \cdot \\
\cdot & = & & & & & \cdot & & & & \cdot \\
S_j & = & a_{1-j} \cdot p_1 & + & a_{2-j} \cdot p_2 & + & a_{3-j} \cdot p_3 & +\ldots+ & a_{i-j} \cdot p_i & +\ldots+ & a_{N-j} \cdot p_N \\
\cdot & = & & & & & \cdot & & & & \cdot \\
\cdot & = & & & & & \cdot & & & & \cdot \\
S_N & = & a_{1-N} \cdot p_1 & + & a_{2-N} \cdot p_2 & + & a_{3-N} \cdot p_3 & +\ldots+ & a_{i-N} \cdot p_i & +\ldots+ & a_0 \cdot p_N
\end{array}
$$

The strength of the "interaction" is characterized by the coefficients a_m where $m = i - j$ .These a_m coefficients are the response of a pole shift p_i on the field change S_j on pole j normalized by the pole shift p_i. Their dimension is therefore [*T/mm*]. The assumption of identical poles is reflected in the fact that they depend only on the difference *i-j* and are assumed to be the same for all poles. The coefficients a_m have been determined experimentally by measuring the response of the magnetic field to a known pole shift (0.5mm) of a known pole (pole #34, the central pole at X=0.) of the upper structure half of the prototype structure. In Fig 2. the effect of this pole shift is shown (dotted line). The full line shows the average field on the poles in the vicinity of pole #34. The index *m* is indicated. Under the pole itself there is the strongest effect, but up to the next four neighbors there is an measurable effect with opposite sign. Integrated over all neighbors this sign change eats up a considerable amount of the correction of the pole itself. The shape of the dotted curve is that of a dipole layer of magnetic surface charges brought on the pole.

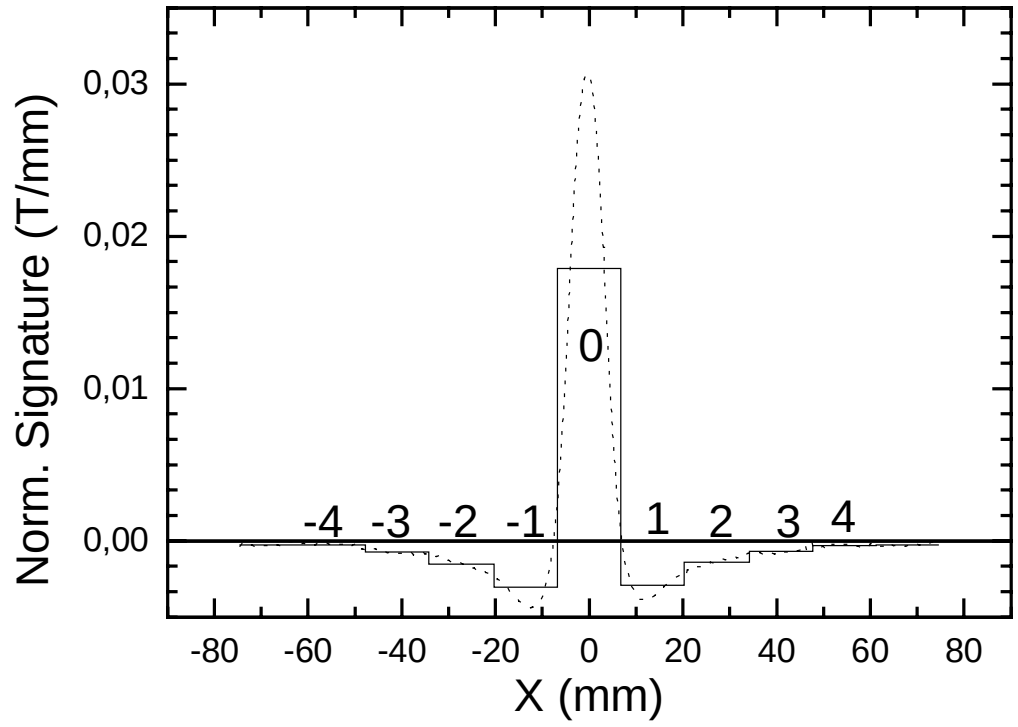

Fig 2 Normalized response of a poleshift of the central pole #34 of the upper magnet structure. Dotted line : Measured difference. Full line: Average field on the poles

It is seen that the interaction on both sides are very similar so that the assumption $a_m = a_{-m}$ holds. We assume the same interaction for all poles so that the coefficient generated from pole #34 are also valid for all other poles. It is also seen that it is sufficient to treat only the four next nearest neighbors. For larger distances the correction becomes negligibly small. The linear system of equations is therefore greatly simplified. Below and above the main diagonal there are only four side diagonals which have to be considered. Using a specialized equation solver for band diagonal systems of equations reduces numerical effort and also minimizes memory requirements dramatically. Large pole numbers can be treated at moderate effort on a PC. Up to 1000 poles has been tried in simulations. Even larger numbers may be possible.

There is no fundamental difference if a structure half, i. e. the top or bottom structure of an undulator or a full magnet structure with closed gap is optimized. Only the a_m coefficients are different and have to be determined for both cases in the proper way as described above. This means that for structure halves the signature of a single pole movement has to be evaluated and in the case of a closed gap the poles in the upper and lower structure have to be moved simultaneously resulting in a local gap change.

For the prototype structure it was found very helpful to seperately optimize the two structure halves first and to do the final fine tuning with the gap closed to the nominal position in a second step. This second step needs only minor additional adjustments.

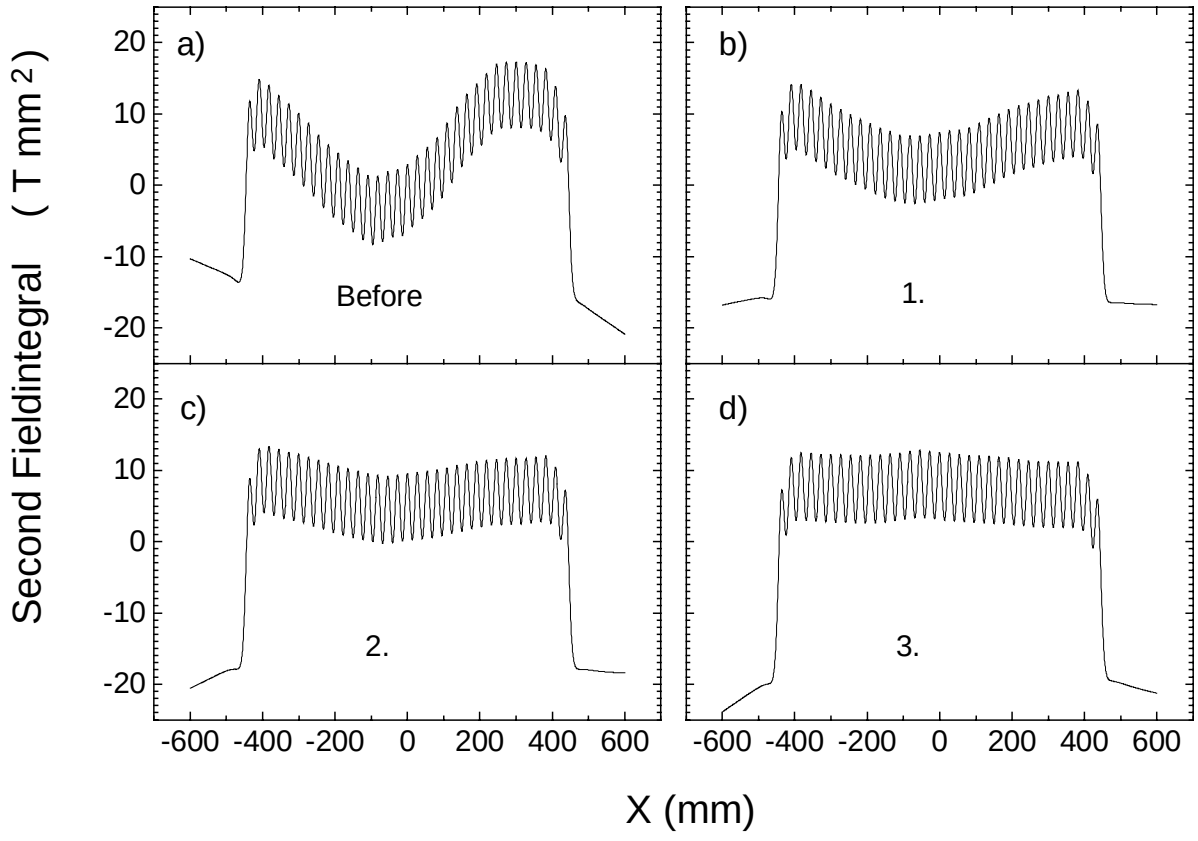

Fig 3 Demonstration of the optimization of the upper structure half in three iteration steps. The 2nd Fieldintegral is shown which is proportional to the beam excursion.
At 300 MeV which will be used for Phase I 10Tmm^2 correspond to 10 μm beam excursion

Results

The 0.9 m long prototype structure was used to test the optimization procedure. Again only the upper structure was used. The field was measured 6mm below the poles corresponding to the nominal electron beam location with respect to the upper structure at a 12mm gap. The resulting second fieldintegral distribution from four iteration steps are shown in Fig.3. The resulting electron beam excursion can be calculated by:

$$z[\mu m] = 587 / \gamma \cdot I_2[Tmm^2] = 0.3 \cdot I_2[Tmm^2] / E_{Kin}[GeV]$$

Where γ is the kinetic electron energy divided by the electron's rest mass energy. Emphasis was put on a straight trajectory in the undulator itself. It is seen in Fig 3 that the endpoles are not adjusted properly. This is of minor importance in this context since they are adjustable anyhow they can be tuned to result in a straight trajectory before and after the undulator. It is seen that within a few Tmm^2 no deviations can be seen corresponding to sub micrometer beam excursions. A full structure with 12mm gap results in twice the field. The fieldintegral deviations in this case therefore will be twice as large. For each interation step the error fields were calculated and the resulting pole height adjustments were calculated. A computer printout was generated containing the pole's number and the amount of adjustment needed on that pole. The amount of adjustments was much larger in the first optimization. For the last iteration step needed only very little correction was needed.

Limitations, Accuracy

The quality of the optimization is influenced by three factors :

1. The accuracy of the field measurements
2. The accuracy of the coefficients a_m
3. The accuracy of the pole height adjustment.

The measurements accuracy was conservatively estimated to be : $\Delta B/B \approx 5.10^{-4}$. In practice it may even be better.

Inaccurate coefficients a_m influence the convergence of the procedure more than the accuracy of the result, which means that more iterations are needed to get the optimized result.

The main source of error is the modest accuracy of local pole height adjustment. ± 5 to 10° of angular accuracy lead to an estimated inaccuracy of the pole height of ± 20 to 40 μm which in turn leads to a field error of about 0.3 - 0.6 % . This is by far the dominant contribution. To improve the accuracy of pole height adjustment one has to measure these changes directly using a suitable dial gauge with micrometer resolution instead of just counting the tuning screw angle. This improvement is underway. With this moderate effort it should be possible to reduce the pole height adjustment error to 5-10 μm or better so that this contribution amounts to less than 0.075 to 0.15% .

References

[1] A. M. Kondratenko, E. L. Saldin, Part. Accel. 10 (1980), 207
[2] R. Bonifacio, C. Pellegrini, L. Narducci, Opt. Comm. 50 (1984), 373
[3] "A VUV Free Electron Laser at the TESLA Test Facility at DESY, Conceptual Design Report" TESLA-FEL Report 95-03, DESY, Hamburg, April 1995
[4] "Tesla Test Facility Linac Design Report" Editor :D. A. Edward , TESLA Report 95-01, Hamburg, March 1995
[5] W. Brefeld, B. Faatz, Y. M. Nikitina, J. Pflüger , J. Roßbach, E.l. Saldin, E.A. Schneidmiller, M. V. Yurkov, Nucl. Instr. and Methods A393 (1997), 119
[6] Y. M. Nikitina, J. Pflüger, Nucl. Instr. and Methods A375 (1996), 325
[7] J. Pflüger, Y. M. Nikitina, TESLA - FEL 96-02, 1996
[8] Y. M. Nikitina, J. Pflüger, TESLA - FEL 96-03, 1996
[9] J. Pflüger, Y. M. Nikitina, Nucl. Instr. and Methods A381 (1996) 554

[10] B. Faatz, J. Pflüger, Y. Nikitina, Nucl. Instr. and Methods A393 (1997), 380
[11] B. Faatz, J. Pflüger, "Sorting strategy for the TTF-FEL undulator magnets" TESLA-FEL report (in preparation)
[12] J.Pflüger, H. Lu, T. Teichmann, Nucl. Instr. and Methods A 407 (1998), 386
[13] R. Stoner, G. Bekefi IEEE Journal of quantum electronics 31,6 (1995) 1158
[14] G. Ramian, Nucl. Instr. and Methods A318 (1992), 225
[15] G. Ramian, J. Kaminski, S.J. Allen, Nucl. Instr. and Methods A393 (1997), 220

Upgrade of the Simulation Code TDA3D

S. Reiche and B. Faatz

Deutsches Elektronen Synchrotron DESY, Notkestraße 85, 22603 Hamburg, Germany

Abstract

The well-known Free Electron Laser (FEL) amplifier simulation code TDA3D has been upgraded to include most of the important features needed for present and future design studies of VUV and X-ray single-pass FELs. A number of bugs have been removed and I/O has been changed and extended to make it more flexible. To features such as wiggler errors, quadrupole misalignment has been added and corrector coils to adjust the beam trajectory. In addition, multi-section undulators can now be simulated with arbitrary (integrated or separated) focusing structures.

1. Introduction

With the design and construction of Free Electron Lasers (FEL), many codes have been developed over the years in order to describe the physics taking place in different regimes (see for example [1]). One such code was a code developed by T.-M. Tran and J.S. Wurtele at MIT, a Three Dimensional Axi-symmetric simulation code (TDA). The physics in this code has been well described as well as suggestions for updates, such as the inclusion of space charge [2]. The code was extended to include non-axisymmetric modes, space charge modes and ion channel focusing [3]. The version of TDA decribed in this paper is based on this code.

There are several new features of importance for future VUV and X-ray FELs. The undulator can be described as modules with driftspaces in between. In addition to the standard FODO lattice, an arbitrary focusing structure can be given as an additional input file. In order to simulate the influence of wiggler errors more realistically, random displacement of quadrupoles has been added. Correction stations, with values and position given in the same input file, are included. Furthermore, the possible parameters that can be given in the output file has been extended and made more flexible.

Table 1. Undulator and optics parameters for the TTF FEL (Phase I at 230 MeV).

Electron beam	
Peak current	500 A
Normalized rms emittance	2π mm mrad
rms energy spread	0.2 %
average beam size	77 μm
undulator	
number of modules	3
length of module	4.5 m
period length	27.3 mm
undulator peak field	0.497 T
length of quadrupoles	136.5 mm
number of quads./module	10
distance between quads.	341 mm
quad. gradient	12.5 T/m

2. Simulation results

As an example, the TTF-FEL parameters have been used to show some typical output. Parameters are given in Table 1. The undulator consists of multiple modules. In Fig. 1, the power growth and the beam radii in both directions are shown. The FODO structure has been integrated into the undulator, with drift section field-free. As can be seen, the variation in the electron beam radius is rather large for this FODO lattice.

The possibility for calculating wiggler errors and quadrupole misalignment, both without and

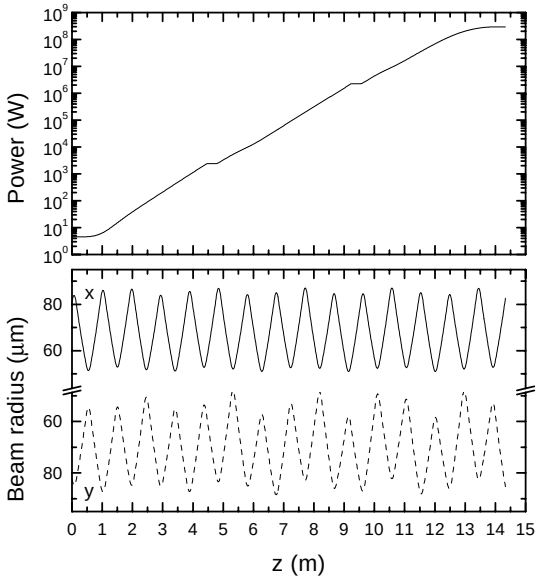

Fig. 1. *Power (top figure) and electron beam radius (bottom figure) along the TTF undulator. Relevant parameters are given in Table 1.*

including correction, is also shown. Comparing the corrected beam with the result in Fig. 1 shows that the power has been reduced by less than a factor of two, but the saturation length stays virtually the same.

Remarks: The Fortran 77 source code as well as the manual can be found on the website:

http://www.desy.de/~tda3d

Acknowledgement: The authors would like to thank P. Pierini and G. Travish for there feedback and usefull discussions.

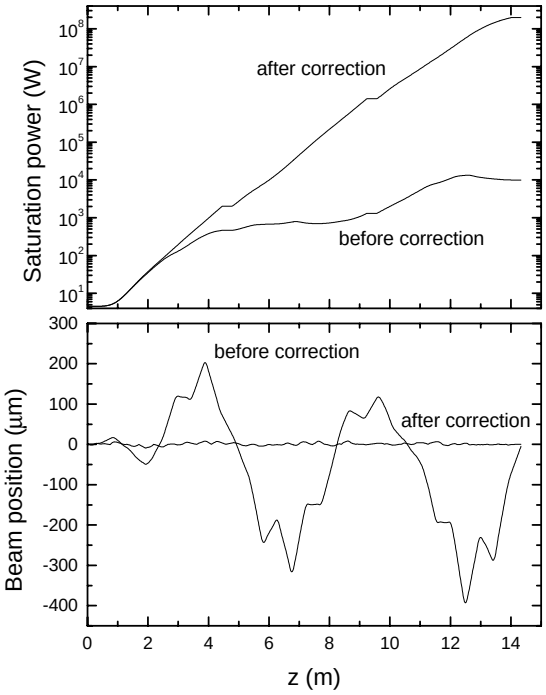

Fig. 2. *Power along the TTF-FEL undulator including undulator dipole field errors (rms value of 0.2%) and quadrupole misalignment (maximum misalignment is* $\pm 20\,\mu m$.*)*

References

[1] G.A. Travish, *Where Do We Stand with High Gain FEL Simulations?*, Towards X-Ray Free Electron Lasers, AIP Conference proceedings 413 Eds. R. Bonifacio and W.A. Barletta, June 1997, Gargnano, Italy.

[2] T.-M. Tran and J.S. Wurtele, *TDA - A Three-Dimensional Axisymmetric Code For Free-Electron-Laser (Fel) Simulation*, Computer Physics Comm. 54 (1989) 263;

[3] P. Jha and J.S. Wurtele, *Three-Dimensional Simulation of a Free-Electron Laser Amplifier*, Nucl. Instr. Meth. **A331** (1993) 477.

GENESIS 1.3 — A Fully 3D Time Dependent FEL Simulation Code

S. Reiche

Deutsches Elektronen Synchrotron, Notkestraße 85, 22603 Hamburg, Germany

Abstract

Numerical simulation codes are basic tools for designing Free-Electron-Lasers (FEL). They are used to study the impact of different parameters, e.g. wiggler errors and external focusing, which allow FEL users to optimize the performance. For faster execution some simulation codes assume radial symmetry or decompose the radiation field into a few azimuthal modes, although then this treatment does not include the full description of the FEL. This contribution describes the new FEL code GENESIS 1.3 which uses a fully 3 dimensional representation of the FEL equations in the paraxial approximation for time dependent and steady state simulations of single-pass free electron lasers. In particular this approach is suitable for cases where the radial symmetry is broken by the electron beam distribution as well as by wiggler errors, betatron motion and off axis injection of the electron beam. The results, presented here, are based on the parameters of the TESLA Test Facility FEL at DESY.

1. Introduction

With the design and construction of Free Electron Lasers (FEL), many codes have been developed [1, 2, 3, 4, 5] over the years in order to describe the physics taking place in different regimes. Recent research is done on the field of Self-Amplified Spontaneous Emission (SASE) FEL [6, 7, 8]. To investigate the properties of this radiation source as well as the extension of SASE FEL's wave length to the VUV or X-ray regime, new codes or extensions of established codes are needed. To cover these aspects and others such as the influence of wakefields, a time dependent code has been developed called GENESIS 1.3.

The algorithm to solve the FEL equation in the paraxial approximation is similar to TDA3D [2]. In fact GENESIS 1.3 is mainly based on TDA3D although major modifications have been made. One of the major improvement is the replacement of the radial mesh with a full Cartesian mesh using the Alternating Direction Implicit (ADI) integration scheme [9] to solve the field equation. This allows the user to study non axi-symmetric cases such as undulator field errors or beam halos.

The basic idea of the extended algorithm for time dependent simulation is to solve the equation for a given slice of the electron bunch and a certain integration length significantly smaller than the gain length before advancing the radiation field to the next slice and replacing it with the radiation field of the trailing slices. This allows only a fractional part of the electron beam and radiation field to be kept in memory.

The source code of GENESIS 1.3 is written in standard ANSI Fortran 77 and can be compiled and linked with common Fortran compilers on any platform. The two restrictions for a successful execution are the support of double complex precision numbers and enough memory for time dependent simulation. During execution the code will read from or write to files using only standard Fortran formats such as sequential or direct access and formatted or unformatted in- and output. GENESIS 1.3 does not support any graphics as output. For visualization of the output data the postprocessor XGENESIS can be used running under the IDL environment [10].

So far the tests which have been made do not show any significant deviation from other well tested codes or analytic results. The CPU time

Electron Beam	
Energy	250/1000 MeV
Energy Spread	0.5/1.0 MeV
Normalized Emittance	2π mm mrad
Ave. Beam Size	60/50 μm
Peak Current	500/2500 A
Bunch Length	250/50 μm
Undulator	
Number of Modules	3/5
Length of Modules	4.5 m
Period Length	2.73 cm
Undulator Peak Field	0.497 T

Table 1. *Parameters of TTF-FEL used for the simulations. If two values are given the first one corresponds to Phase I of the TTF-FEL, the second to Phase II.*

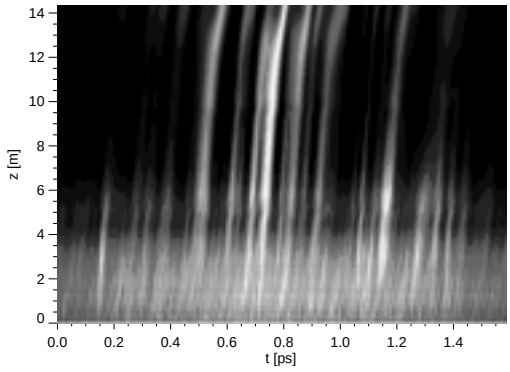

Fig. 1. *Radiation power of TTF-FEL (Phase I) versus longitudinal position in the electron bunch (horizontal axis) and undulator (vertical axis). The radiation pulse is normalized to unity for all undulator positions to exclude the dominant exponential growth of the radiation field.*

consumption is moderate and steady state simulation, even on Personal Computers, will run in the range of minutes. For time dependent simulation the CPU time scales linearly with the number of macroparticle slices.

To illustrate the application regime of GENESIS 1.3, only few important examples will be shown in this paper. All simulations are based on the parameters of the TESLA Test Facility Free Electron Laser (TTF-FEL) which are listed in Table 1.

2. Time Dependent Simulation

One of the most important applications of time dependent codes is the simulation of SASE FEL's. Following the algorithm described in [11] spontaneous emission seeds the FEL amplifier instead of

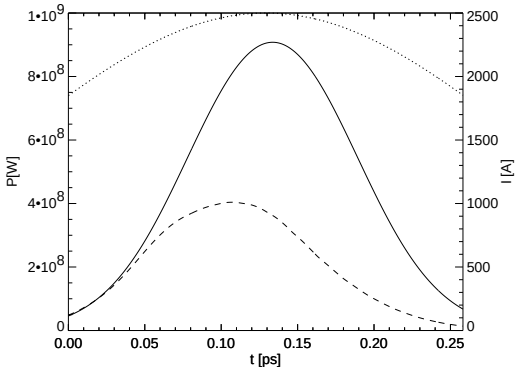

Fig. 2. *FEL radiation of TTF-FEL (Phase II) including energy losses of the electron beam due to wakefields (dashed line). The power of the radiation pulse is significantly decreased in comparison to the FEL radiation excluding the effect of wakefields (solid line). Both simulations used the same set of parameters such as the same longitudinal beam current profile (dotted line) and same seeding field.*

an external seeding field commonly used in steady state simulations. As an example a compact representation of the result for a single run is shown in Fig. 1 using the parameters of the TTF-FEL Phase 1 (see Table 1). For each longitudinal position in the undulator (vertical axis) the radiation pulse (horizontal axis) is normalized in such a way that the maximum always has the same value. In this way the structure of the pulse is clearly visible for any position in the undulator. Otherwise the exponential growth of the SASE FEL amplification process will dominate. It is seen that the number of spikes is decreasing along the undulator and the contrast is enhanced. Both effects arise due to growing longitudinal and transverse coherence.

To demonstrate another application regime for time dependent simulation, the influence of wakefields on the performance of the TTF-FEL is investigated. This is of particular concern for Phase II with its short rms bunch length of 50 μm. The geometric and electromagnetic properties of the beam pipe provide three major sources for wakefields: conductivity, surface roughness and geometric changes of the beam pipe along the undulator. For the parameters of the TTF-FEL all three wake potentials have nearly the same amplitude but different shapes [12]. For a time dependent simulation covering a length of about 100 μm around the peak current, the gradient of the total wake potential varies between -100 keV/m and 30 keV/m.

Because most electrons are shifted away from the FEL resonant condition due to the wakefields,

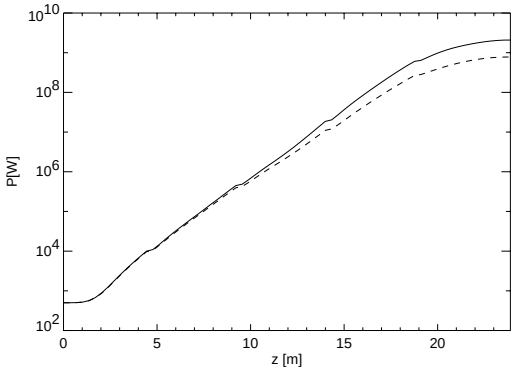

Fig. 3. *Radiation power versus undulator position including (dashed line) and excluding (solid line) wakefields.*

the total gain is significantly reduced. For a position close to saturation the radiation pulse is plotted in Fig. 2. In contrast to the undisturbed FEL performance the maximum of the radiation pulse is trailing behind the maximum of the beam current distribution. The reason is that slippage of the radiation field has less influence than the detuning of the electron beam which is stronger in the front part of the electron beam.

In Fig. 3 the radiation power with and without wakefields taken into account is plotted as a function of the longitudinal position in the undulator. It is seen that the power reduction due to wakefields is larger in the last part of the undulator due to the accumulated energy losses of the electron beam. The saturation length remains nearly unchanged and is reached in this case when most of the beam is completely detuned.

3. Non Axi-Symmetric Simulation

As an example of broken axi-symmetry the case of undulator field errors for the TTF-FEL (Phase I) is simulated [13].

For a relative rms error of 0.3 % for the field errors the radiation distribution at two positions within the undulator is presented in Fig. 4. At these positions the electron beam centroid was deflected from the undulator axis and bent backwards due to strong focusing. The radiation field, unable to follow the rapid motion of the electron beam, becomes distorted. The steeper edges of the radiation field distribution induce a larger diffraction in addition to a reduced gain guiding because the electron beam position has changed transversely. The lower plot of Fig. 4 shows such a large diffracted part of the radiation field.

The FEL gain is also reduced by other effects

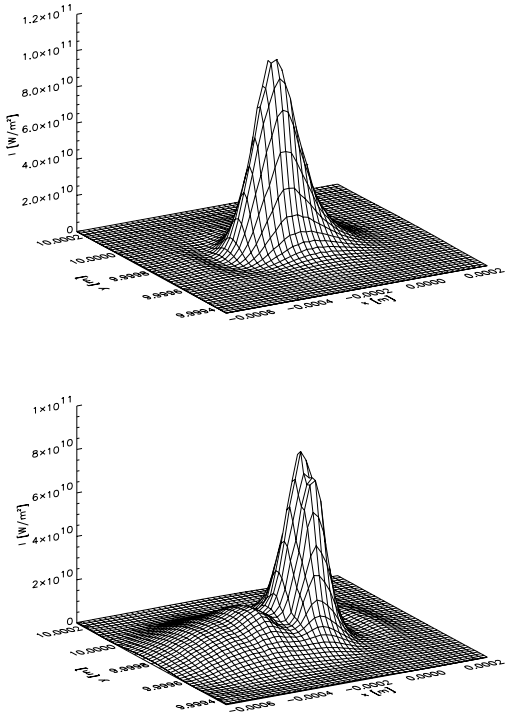

Fig. 4. *Intensity of radiation field for FEL simulation including magnetic field errors. The data shows a typical case where the electron beam is kicked towards one direction in the horizontal plane (upper plot) and bent back towards the undulator axis (lower plot).*

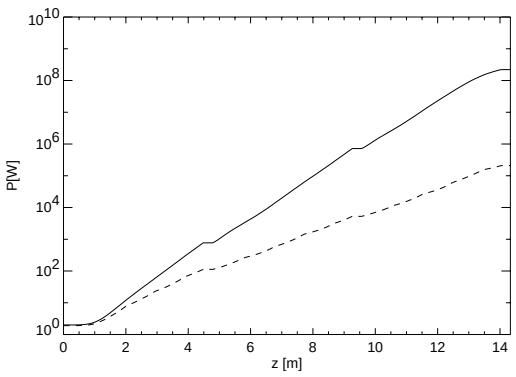

Fig. 5. *Radiation power versus undulator position for the TTF FEL (Phase I) including magnetic field errors (dashed line). For the calculation 400 independent runs are averaged with a relative rms field error of 0.3%. The undisturbed FEL performance is shown by the solid line.*

such as loss of the synchronization condition of the electron beam and radiation field. For this case the coherent transverse kick reduces the longitudinal velocity of the electron beam. The average power gain versus longitudinal position in the undulator is shown in Fig. 5 with a saturation power reduced by nearly 3 orders of magnitudes relative to the undisturbed motion of the electron beam.

4. Conclusion

Although several FEL codes already exist, there is an increasing demand to cover new aspects of FEL performance in order to keep up with the advance research. GENESIS 1.3 contains several new features and allows the user to describe the problem in a more flexible manner. Even for cases which are not covered by the standard features of GENESIS 1.3, the user has the option to modify the source code for his own purposes, because GENESIS 1.3 is distributed free. Thus GENESIS 1.3 provides a new and useful tool for FEL-physics.

5. Acknowledgment

The author would like to thank B. Faatz, E.L. Saldin, E.A. Schneidmiller, H. Schlarb and M.V. Yurkov for their useful discussions.

References

[1] G.A. Travish, Proceeding of the X-ray workshop, June 1997, Gargnano, Italy.

[2] T.-M. Tran and J.S. Wurtele, Computer Physics Comm. 54 (1989) 263.

[3] E.T. Scharlemann et al., Nucl. Instr. Meth. **A250**(1986) 150.

[4] W.M. Fawley, CBP Tech Note-104 (1995).

[5] E.L. Saldin, et al. *Three dimensional, time-dependent FEL simulation code S&D-3T*, presented at this conference.

[6] M. Hogan et al., *Measurement of Gain Larger Than* 10^5 *at* $12\mu m$ *in a SASE FEL*, presented at this conference.

[7] DESY Print TESLA-FEL 95-03, Hamburg, DESY, 1995.

[8] R. Tatchyn et al., Nucl. Inst. Meth. **A375** (1996) 274.

[9] W.H. Press et al., *Numerical Recipes in Fortran 77*, Cambridge University Press (1992).

[10] *IDL - Interactive Data Language*, Research System Inc.

[11] C. Penman and B.W.J. McNeil, Opt. Commun. **90** (1992) 82.

[12] M. Dohlus et al., DESY Print TESLA-FEL 98-02, Hamburg, DESY, 1998.

[13] B. Faatz et al., Proceeding of the FEL 96 conference, (1997) 277

A High Average Power UV FEL Amplifier at a 1 GeV Superconducting Linear Accelerator at the TESLA Test Facility at DESY

E.L. Saldin[a], E.A. Schneidmiller[a], M.V. Yurkov[b]

[a] *Automatic Systems Corporation, 443050 Samara, Russia*

[b] *Joint Institute for Nuclear Research, Dubna, 141980 Moscow Region, Russia*

Abstract

This paper presents analysis of a possibility of constructing a high power ultraviolet free electron laser at a 1 GeV superconducting linear accelerator being under construction at the TESLA Test Facility (TTF) at DESY. The MOPA scheme is studied when the radiation from a tunable master oscillator is amplified in the FEL amplifier with tapered undulator. The average and the peak radiation power at the exit of the FEL amplifier are about 7 kW and 220 GW, respectively. Possible applications of such a powerful source of coherent UV radiation are discussed.

1. Introduction

A 1 GeV superconducting linear accelerator being under construction at the TESLA Test Facility (TTF) at DESY will produce electron beam with a high average and peak power, low energy spread and emittance. The main practical application of this accelerator is to use it for driving the soft X-ray free electron laser [1]. In this paper we perform design consideration of another possible option for the TTF — a high power UV free electron laser [2]. It is supposed to install an additional FEL beamline in the same tunnel in parallel with the soft X-ray FEL (see Fig. 1). UV FEL will use the same electron beam as an X-ray FEL, thus providing minimal interference between these two options. It will be constructed as a Master Oscillator Power Amplifier (MOPA) scheme. Radiation from a dye laser system ($P_{\rm av} \sim 10$ mW, $P_{\rm peak} \sim 5$ kW, $\lambda \simeq 200 - 350$ nm) pumped by Nd glass laser with subsequent using nonlinear optical elements [2] will be amplified in the FEL amplifier with a tapered undulator providing peak and average output power up to 220 GW and 7 kW, respectively.

Installation of a powerful UV FEL at the TESLA Test Facility can extend significantly scientific potential of researches at the TTF revealing unique possibility for constructing of a high-intensity gamma-source, for constructing the test facility for the next generation linear colliders and for industrial applications.

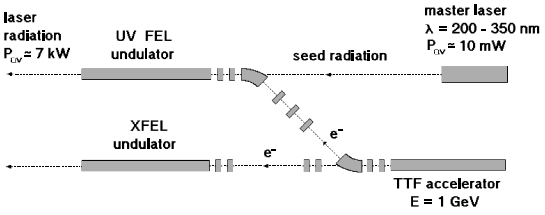

Fig. 1. Scheme of the UV FEL at the TESLA Test Facility.

2. FEL amplifier

Starting point of the design are the project parameters of the electron beam from the TTF accelerator (see Table 1). Undulator period has been chosen to be equal to 7 cm. At the operating wavelength of the FEL amplifier around 200 nm the peak value of the magnetic field is about 1 T. The peak power of the master laser (5 kW) exceeds by two orders of magnitude the effective power of the shot noise in the electron beam. Main physical effects influencing the operation of the FEL amplifier in this region of parameters

are the diffraction effects, the space charge effects and the slippage effect. Optimization of the parameters of the FEL amplifier has been performed with nonlinear, three-dimensional, time-dependent simulation code FAST which takes into account all these effects [3].

Saturation of the radiation power in the FEL amplifier occurs due to the energy losses by the particles which fall out of the resonance with the electromagnetic wave. Nevertheless, effective amplification of the radiation is possible in the nonlinear regime by means of using a tapered undulator [4]. Calculations based on the steady-state theory show that at the length of the undulator of 30 m, the efficiency of the UV FEL amplifier at the TESLA Test Facility can reach the value of 10 %. Nevertheless, at such a length of the undulator one should take into account the slippage effect. Kinematic slippage of the radiation with respect to the electron bunch is about 90 μm which is comparable with the length of the electron bunch. So, steady-state approach can be used only for rough estimations, and parameters of the FEL amplifier should be optimized using time-dependent approach.

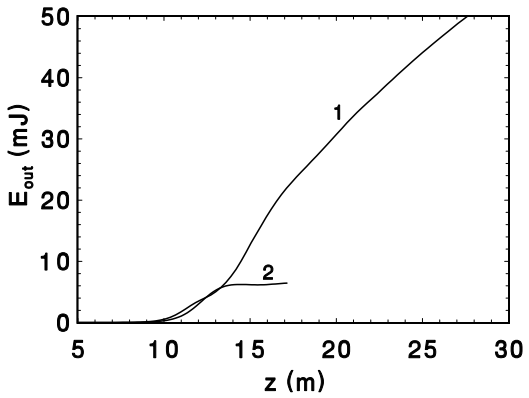

Fig. 2. Energy in the radiation pulse versus the length for the FEL amplifier with tapered undulator (curve 1) and for the FEL amplifier with untapered undulator (curve 2).

Optimized parameters of the FEL amplifier are presented in Table 1. The length of untapered section of the undulator is equal to 12 m. The field in the tapered section is reduced by a linear law from 0.99 T down to the value of 0.87 T at the end of the undulator of 28 m. Figure 2 presents evolution along the undulator length of the energy in the radiation pulse. In Fig. 3 we present the time structure of the radiation pulse at the exit of the undulator. We obtain that the peak radiation power of about 220 GW is close to that predicted by the steady-state calculations. The conversion efficiency (ratio of the energy in the radiation pulse to the energy in the electron pulse) is equal to

Table 1. Parameters of the UV FEL with tapered undulator

Accelerator	
Energy	1 GeV
Mode of operation	quasi-CW
Repetition rate	10 pps
Macropulse duration	800 μs
Number of bunches per macropulse	14400
Micropulse repetition rate	18 MHz
Charge per bunch	1 nC
Average power in the electron beam	144 kW
Peak current	2.5 kA
Bunch length (RMS)	50 μm
Normalized emittance (RMS)	2 mm mrad
Energy spread (RMS)	1 MeV
Undulator	
Type	Planar
Period	7 cm
Maximal field (entr./exit)	0.99 T / 0.87 T
Total length	28 m
Length of untapered section	12 m
Beam size in the undulator (RMS)	83 μm
Radiation	
Wavelength	200 – 350 nm
Dispersion	Diffraction limited
Spot size at the undulator exit (HWHM)	170 μm
Angular divergence (HWHM)	0.13 mrad
Pulse duration (FWHM)	230 fs
Repetition rate	10 pps
Macropulse duration	800 μs
Number of pulses per macropulse	14400
Micropulse repetition rate	18 MHz
Peak output power	220 GW
Average power	7.2 kW
Efficiency	5 %

5 %. Average power of the radiation from the FEL amplifier with tapered parameters is equal to 7.2 kW. Analysis of the distribution of the beam power losses along the electron beam (see Fig. 3) shows that the radiation is produced mainly by the front fraction of the electron pulse which is a consequence of the slippage effect mentioned above. On the other hand, one can see that actual slippage of the radiation pulse (about 30 μm) is significantly less than the kinematic slippage (about 100 μm). This difference is connected with the interaction of the radiation with the electron beam leading to the dynamic change of the phase of the radiation field. As a result, group velocity of the radiation pulse, $\partial\omega/\partial k$, becomes less than the velocity of light. We see that this effect reveals the possibility to achieve high extraction efficiency even in the case of a short electron bunch with respect to the kinematic slippage distance.

Phase analysis of the particles shows that the electrons of the front and of the middle parts of the beam

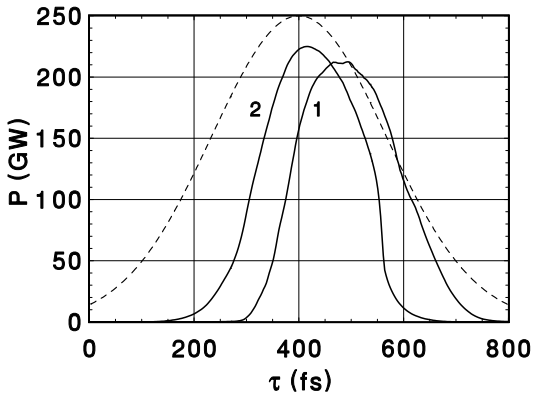

Fig. 3. Time structure of the radiation pulse at the exit of the FEL amplifier with tapered undulator (curve 1) and of the power loss in the electron bunch (curve 2). Dashed line is the longitudinal profile of the electron bunch (maximal value of the beam current is equal to 2.5 kA).

are well separated into two fractions, of about 70 % of the electrons are trapped in the regime of coherent deceleration (see Fig. 4). The electrons of the back part of the beam fall out the regime of coherent deceleration due to the slippage of the radiation. In Fig. 5 we present energy distribution in the electron beam at the exit of the undulator. It is seen that the energy spectrum of the spent beam is rather wide, of about 12 %.

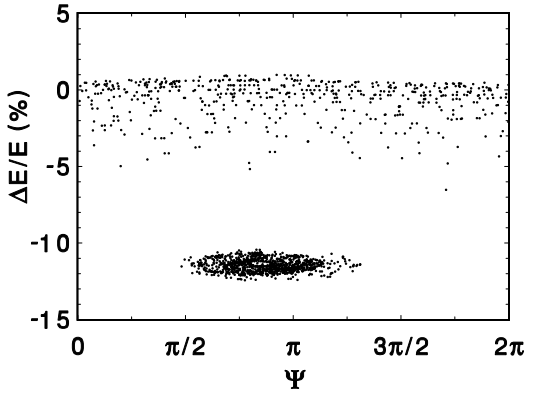

Fig. 4. Phase distribution of the particles in the middle of the electron bunch. Total efficiency of the FEL amplifier is equal to 5 %.

The directivity diagram of the radiation in far diffraction zone (see Fig. 6) is an important characteristics for users of the proposed UV radiation source. The width of the angle distribution is visibly smaller than that of the FEL amplifier operating at the saturation [2] which is connected with the increasing of the radiation spot size inside the undulator. Also, there are distortions of the directivity diagram connected with complicated shift of the radiation field phase along the transverse coordinate.

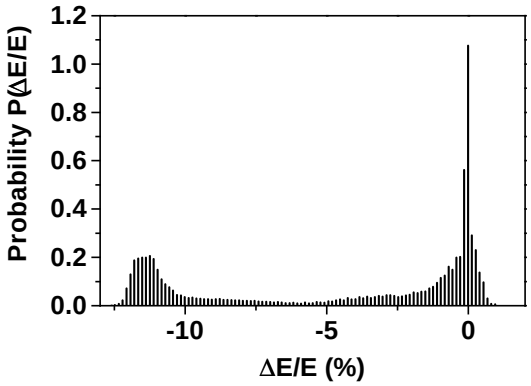

Fig. 5. Energy distribution of the electrons at the exit of the FEL amplifier with tapered undulator. Total efficiency of the FEL amplifier is equal to 5 %.

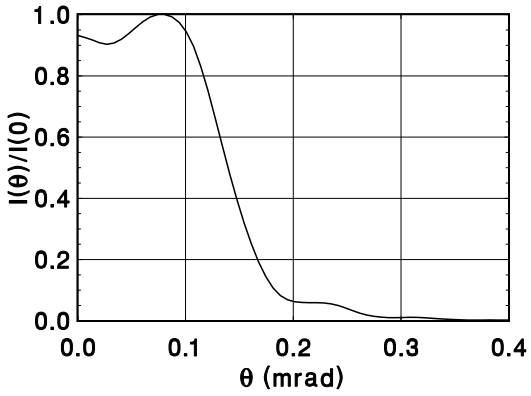

Fig. 6. Directivity diagram of the radiation intensity in far zone for the FEL amplifier with tapered undulator. Total efficiency of the FEL amplifier is equal to 5 %.

In Fig. 7 we present the dependence of the energy in the radiation pulse as a function of the deviation of the wavelength of the master laser from exact FEL resonance. This characteristic can be simply rescaled to the case of the energy deviation as $\Delta\mathcal{E}/\mathcal{E} = \Delta\lambda/2\lambda$. It is seen that at the designed stability of the energy of the accelerator ($\sim$ 0.1 %) the fluctuations of the energy in the radiation pulse are about one per cent. The requirement to the stability of the frequency of the master laser is also extremely loose.

Analysis of the parameters of the UV FEL amplifier beyond the project parameters of the TESLA accelerator shows that it will operate reliably even at the value of the emittance exceeding the project value by several times. There is also significant safety margin (by a factor two) with respect to the value of the instantaneous energy spread. So, we can conclude that

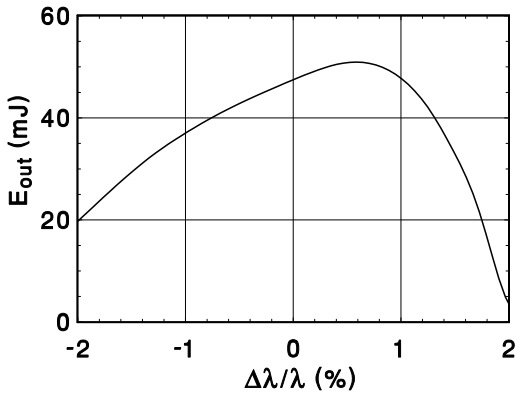

Fig. 7. Dependence on the wavelength deviation from exact FEL resonance of the energy in the radiation pulse of the FEL amplifier with tapered undulator. Total efficiency of the FEL amplifier is equal to 5 %.

the ultraviolet free electron laser at the TESLA Test Facility will operate reliably with large safety margins with respect to critical parameters of the accelerator.

3. Possible applications

A powerful UV FEL at the TESLA Test Facility can provide unique possibility for constructing of a polarized, monochromatic gamma-source with ultimate yield up to 10^{12} gamma-quanta per second and for constructing the test facility for the next generation linear colliders [2, 5]. Gamma-quanta will be produced by Compton scattering of UV radiation on 1 GeV electron beam.

Also, a high average power UV FEL has perspective for industrial applications. During last few years the problem of industrial applications of a kW level power FELs intensively discussed in the FEL community. Recently this discussions have been realized in a project of industrial FEL which is supported by a consortium of industrial firms including DuPont, 3M, Xerox, AT&T and IBM [6]. It is interesting to notice that this project is also based on a superconducting accelerator. The chosen FEL configuration is an oscillator. Since this device has low efficiency, the designers of the project have chosen the way of electron recuperation in order to increase the net efficiency of the laser. Another significant problem to be solved is that of the optical resonator connected with a high level of the intracavity power.

In this paper we point at the possibility of using an alternative approach for constructing a high power UV FEL. It consists in using a Master Oscillator — Power Amplifier (MOPA) scheme. A high efficiency FEL amplifier with tapered undulator allows one to overcome significantly the level of the peak and the average output power attainable in an FEL oscillator. This is due to the fact that there are no problems with the mirrors in the high gain FEL amplifier. Also, there is no limitation on the way of decreasing the operating wavelength or expanding it beyond the harmonics of the dye laser band. Low powerful FEL oscillator can be used in this case as a master laser. Comparison with CEBAF project (see Fig. 8 and ref. [6]) indicates that potential of the UV FEL at the TESLA Test Facility for possible industrial applications should be studied in detail, too.

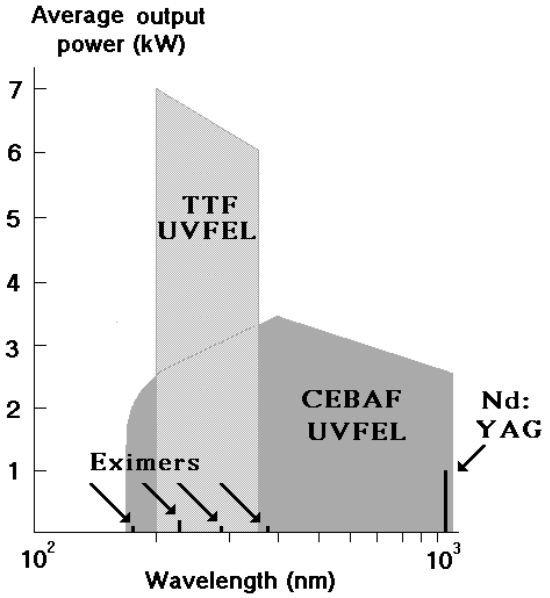

Fig. 8. Operating ranges of the CEBAF UV FEL and of the UV FEL at the TESLA Test Facility

References

[1] J. Rossbach, Nucl. Instrum. and Methods **A375**(1996)269.

[2] C. Pagani, E.L. Saldin, E.A. Schneidmiller and M.V. Yurkov, " Design considerations and analysis of potential applications of a high power ultraviolet FEL at the TESLA Test Facility at DESY", DESY print, TESLA-FEL 98-03, Hamburg (1998).

[3] E.L. Saldin, E.A. Schneidmiller and M.V. Yurkov, "FAST: Three dimensional, time-dependent FEL simulation code S&D-3T", presented at this Conference.

[4] N. Kroll, P. Morton and M. Rosenbluth, SRI Rep. JSR-79-01
IEEE J. Quantum Electron. **QE-17**(1981)1436.

[5] C. Pagani, E.L. Saldin, E.A. Schneidmiller and M.V. Yurkov, "An FEL based high intensity gamma-source at the TESLA test facility at DESY", presented at this Conference.

[6] G.R. Neil, S.V. Benson, H.F. Dylla and H. Liu, Nucl. Instrum. and Methods **A358**(1995)159.

Formation of the Transverse Coherence in SASE FEL

E.L. Saldin[a], E.A. Schneidmiller[a], M.V. Yurkov[b]

[a] *Automatic Systems Corporation, 443050 Samara, Russia*

[b] *Joint Institute for Nuclear Research, Dubna, 141980 Moscow Region, Russia*

Abstract

This report presents first fully three-dimensional study of the amplification process in the Self Amplified Spontaneous Emission (SASE) free electron laser. Investigations are based on the data obtained with three-dimensional, time-dependent FEL simulation code FAST. Analysis of obtained data shows that statistical properties of the radiation can be described with the Gaussian statistics. In particular, fluctuations of the instantaneous radiation intensity in one space point follows the negative exponential law, while the finite-time integrals of the radiation intensity (both in space and in time) follows the gamma-distribution. Numerical examples presented in the paper correspond to 70 nm SASE FEL being under construction at the TESLA Test Facility at DESY.

1. Introduction

The process of amplification in the SASE FEL starts from the shot noise in the electron beam. Since the FEL amplifier is a narrow bandwidth device, it selects from the shot noise and begins to amplify only a narrow fraction of the fluctuation spectrum. During the amplification process the longitudinal coherence of the radiation is increased and the process of the formation of the transverse coherence takes place. The process of formation of the longitudinal coherence can be studied in the framework of the one-dimensional theory, since it is mainly connected with the slippage effect. Reliable analytical and numerical methods allowed to study this effect in details [1]. As for the investigation of the transverse coherence formation, there are only qualitative predictions based on the results of the steady-state approximation. Namely, in the linear high-gain limit the radiation of the electron beam in the undulator may be represented as a set of modes having different growth rates. At sufficient length of the undulator the fundamental mode should survive having the maximal gain. On the other hand, the gain in the SASE FEL till it reaches the saturation has limited value and one should perform quantitative study if such a single-mode asymptote will be realized in practical device. At present there are no reliable analytical approaches giving this quantitative results, and the information on the process of the transverse coherence formation can be obtained only with fully three-dimensional, time-dependent simulation codes. Recently it has been reported that two such codes, FAST and GENESIS, have been issued [2, 3].

In this paper we present numerical study of the process of amplification in the SASE FEL using the numerical simulation code FAST [2]. To be specific, we present the numerical examples for the 70 nm SASE FEL being under construction at the TESLA Test Facility at DESY (see Table 1) [4]. The obtained results are used for the planning of the experiments on the characterization of the photon beam from this FEL [5].

2. Results of numerical simulations

Numerical simulations have been performed with three-dimensional, time-dependent FEL simulation code FAST [2]. Parameters of the simulations have been chosen to achieve the accuracy of simulation about one per cent. The size of the longitudinal slice is equal to four radiation wavelengths, the number of the radial and azimuthal divisions is equal to 16 and 50, respectively, and the number of azimuthal modes for the radiation field calculations has been set to nine. The numerical simulation code produces the matrixes for the field values in the Fresnel diffraction zone. Typical output results for the instantaneous power flux density inside the undulator are presented in Fig. 1.

Table 1. Parameters of the 70 nm SASE FEL at DESY

Electron beam	
Energy, $\mathcal{E}_0$	300 MeV
Peak current, I_0	500 A
rms bunch length, σ_z	250 μm
Normalized rms emittance , ϵ_n	2π mm mrad
External β-function,	100 cm
Number of bunches per train	7200
Repetition rate	10 Hz
Undulator	
Type	Planar
Length of undulator, L_w	13 m
Period, λ_w	2.73 cm
Peak magnetic field, H_w	4.97 kGs
Radiation	
Wavelength, λ	71.4 nm
Power averaged over pulse	300 MW
Flash energy	0.05 mJ
Average power	45 W

Using the data for the radiation field in the near zone the post-processor code can calculate the distributions of the radiation intensity in the far zone (see Fig. 2).

The process of the amplification starts from the shot noise, and at the beginning of the amplification process there are many transverse radiation modes contributing to the FEL power. At increasing the undulator length the higher modes begin to give less contribution and the field distribution tends asymptotically to that predicted by the steady-state theory [6, 7].

Integration of the radiation flux density across the electron beam allows one to obtain the time structure of the radiation pulse (see Fig. 3). In Fig. 4 we present the corresponding probability distribution of the radiation power obtained from a large number of statistical runs. It is seen that the probability distribution follows the gamma distribution

$$p(P) = \frac{M^M}{\Gamma(M)} \left(\frac{P}{< P >}\right)^{M-1} \frac{1}{< P >} \exp\left(-M \frac{P}{< P >}\right) ,$$

where $\Gamma(M)$ is the gamma function of argument M. Parameter of the distribution is equal to $M = 1/\sigma^2$, where $\sigma^2 = \langle P^2 - \langle P \rangle^2 \rangle / \langle P \rangle^2$ is the normalized dispersion of the distribution of the instantaneous radiation power. In the case under study the physical sense of parameter M is the average number of transverse radiation modes.

Statistical simulations allows us to perform quantitative description of this transverse coherence formation process in terms of the average number of the transverse radiation modes, M (see Fig.5). At increasing the length of the undulator the number of the transverse radiation modes approaches asymptotically to one. Analysis of this plot shows that we can expect

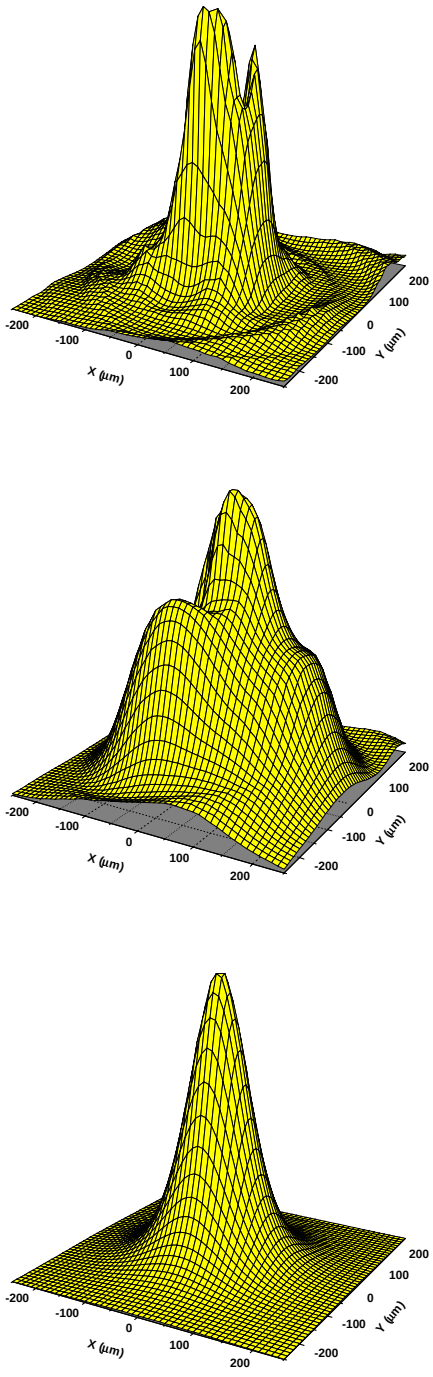

Fig. 1. Distribution of the instantaneous power flux density in the near zone at the undulator length of 2 m, 4.5 m and 8 m (upper, middle and lower plot, respectively).

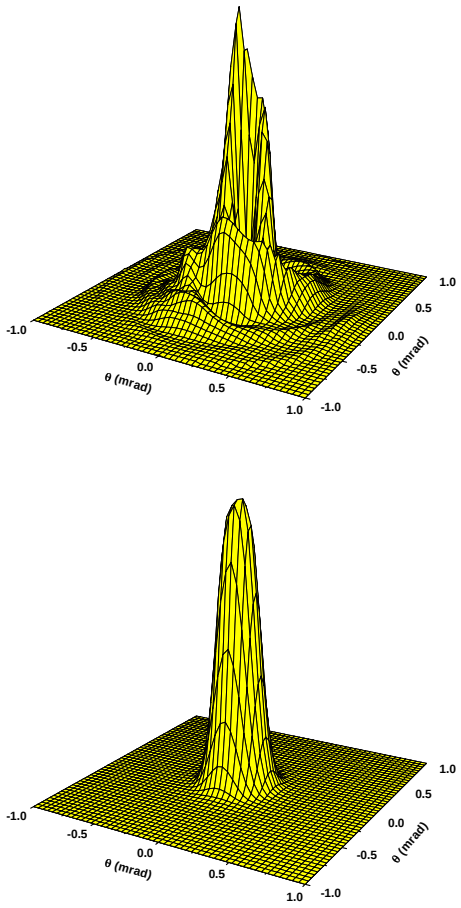

Fig. 2. Directivity of the instantaneous radiation intensity in far zone at the undulator length of 2 m, 4.5 m and 8 m (upper and lower plot, respectively).

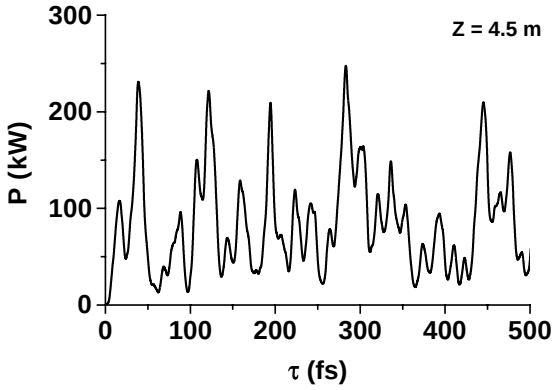

Fig. 3. Temporal structure of the radiation pulse at the undulator length of 4.5 m.

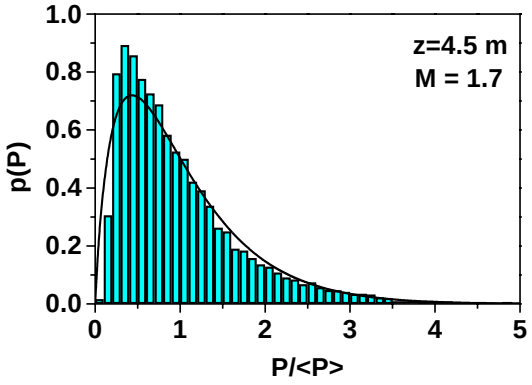

Fig. 4. The probability distribution of the instantaneous radiation power at the undulator length of 4.5 m.

almost full transverse coherence of the radiation at the exit of the 70 nm SASE FEL at DESY.

The values of practical interest is the saturation length and the saturation power. Since the temporal structure of the radiation is a spiky one (see Fig. 3), it is reasonable to calculate the value of the radiation power averaged over many pulses. In Fig. 6 we present the dependency of the averaged radiation power on the undulator length. The calculations have been performed with the nonlinear simulation code for negligibly small energy spread. It is seen that with such an optimistic scenario one one can expect to reach the saturation in the 70nm SASE FEL at DESY. Analysis of the plot in Fig. 6 allows also to calculate the value of the "effective" shot noise power to be used in the steady-state simulation code is of about 10 W. The dashed curve in Fig. 6 presents the results of the steady-state simulations. It is seen that the steady-state simulations give reliable estimation for the values of the saturation length and the average saturation power for the parameters of the 70 nm SASE FEL at DESY.

Acknowledgments

We are grateful to B. Faatz, J. Feldhaus, G. Materlik, J. Pflüger, S. Reiche, J. Roßbach and J.R. Schneider for many useful discussions.

References

[1] E.L. Saldin, E.A. Schneidmiller and M.V. Yurkov, Opt. Commun. **148**(1998)383.

[2] E.L. Saldin, E.A. Schneidmiller and M.V. Yurkov, "FAST: Three-dimensional Time-Dependent FEL Simulation Code", Presentation at the 20th FEL Conference, Williamsburg, 1998.

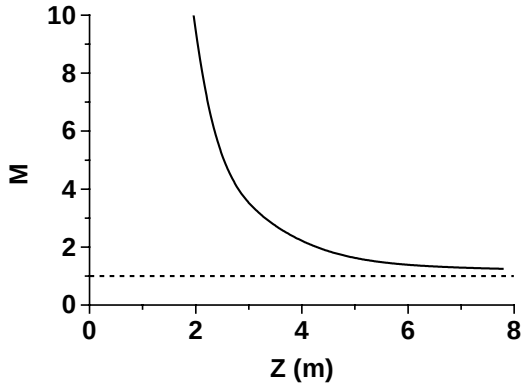

Fig. 5. The dependence of the number of transverse modes, M, versus the undulator length.

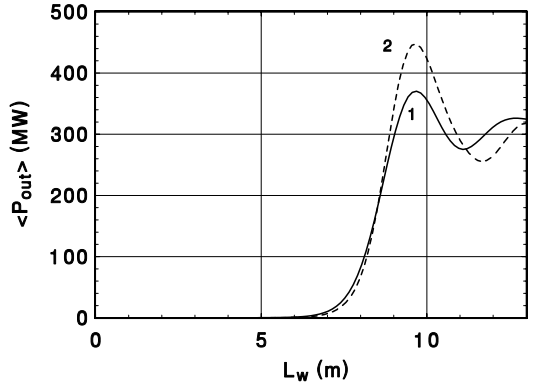

Fig. 6. The dependence of the radiation power averaged over the pulse length on the undulator length. Dashed curve presents the results of the steady-state simulation with the input power of 10 W.

[3] S. Reiche, "GENESIS 1.3- A Fully 3D Time Dependent FEL Simulation Code", Presentation at the 20th FEL Conference, Williamsburg, 1998.

[4] W. Brefeld et al., "Parameter Study on Phase I of the VUV FEL at the TESLA Test Facility", DESY Print TESLA-FEL 96-13, to be published in Nucl. Instrum. and Methods (Proc. of 19th FEL Conf.).

[5] Proceedings of the Workshop on the Characterization of the Photon BeamEmitted by the VUV SASE FEL at DESY (DESY, Hamburg, April 2-3, 1998), DESY, Hamburg, 1998.

[6] E.L. Saldin, E.A. Schneidmiller and M.V. Yurkov, Opt. Commun. **97**(1993)272.

[7] E.L. Saldin, E.A. Schneidmiller and M.V. Yurkov, Phys. Rep. **260**(1995)187.

FAST: Three-dimensional Time-Dependent FEL Simulation Code

E.L. Saldin[a], E.A. Schneidmiller[a], M.V. Yurkov[b]

[a] *Automatic Systems Corporation, 443050 Samara, Russia*

[b] *Joint Institute for Nuclear Research, Dubna, 141980 Moscow Region, Russia*

Abstract

In this report we briefly describe three-dimensional, time-dependent FEL simulation code FAST. The equations of motion of the particles and Maxwell's equations are solved simultaneously taking into account the slippage effect. Radiation fields are calculated using integral solution of Maxwell's equations. Special technique has been developed for fast calculations of the radiation field reducing drastically required CPU time. As a result, the developed code allows one to use personal computer for time-dependent simulations. The code allows one to simulate the radiation from the electron bunch of any transverse and longitudinal bunch shape; to simulate simultaneously external seed with superimposed noise in the electron beam; to take into account energy spread in the electron beam and the space charge fields; and to simulate high-gain, high-efficiency FEL amplifier with tapered undulator. It is important, that in the developed code there are no significant memory limitations and the electron bunch of any length can be simulated.

1. Introduction

Complete calculation of the parameters of the FEL amplifier can be performed only with numerical simulation codes. At present there are several numerical simulation codes calculating the amplification process in the FEL amplifier using the steady-state approximation. Such an approximation describes rather well the case when the FEL amplifier is seeded by the monochromatic external radiation and when the slippage effect can be neglected. Such a simplification allows one to simulate the electron beam with one slice equal to the radiation wavelength, thus reducing significantly the requirements to the computer resources. Nevertheless, the steady-state simulations do not provide a correct result when the slippage of the radiation is comparable with the length of the electron bunch. The steady-state code can not be used in principle for the simulations of the FEL amplifier starting from the shot noise (SASE FELs), and complete simulation of the SASE FELs can be done only with a fully three-dimensional, time-dependent simulation code.

Recently it has been reported on the development of one-dimensional, time dependent simulation codes which revealed the possibility to perform detailed investigation of the process of formation of the longitudinal coherence in the SASE FELs. Nevertheless, the one-dimensional approximation omits an essential effect of the diffraction of the radiation giving only rough estimation of the SASE FEL parameters. Complete simulation of the physical process in the SASE FEL can be done only with a three-dimensional, time dependent simulation code. Unfortunately, the progress in this field is rather limited, and the main reason for this is due to limited possibilities of the computers.

In this paper we report on the development of a fast three-dimensional, time-dependent simulation code FAST. The ideas implemented during the construction of this code allowed to reduce significantly the requirements to the computer and the simulations of actual devices can be performed using a conventional personal computer.

2. General approach

Time-dependent simulations of the FEL amplifier should be performed by simultaneous solutions of Maxwell's equations and the equations of motion of the electrons. Nevertheless, the problem formulated in such a general form can not be implemented in the simulation code and some physical approxima-

tion should be made. Here it is reasonable to remember that the free electron laser is a resonance device amplifying the radiation within the narrow bandwidth. Using resonance approximation we present the transverse beam current density is presented as $j_1(\vec{r},t) = \tilde{j}_1(\vec{r},t)\exp(i\omega(z/c-t)) + C.C.$, where ω corresponds to the resonance FEL frequency and $\tilde{j}_1(\vec{r},t)$ is the slowly varying complex amplitude. The radiation field is also presented in the resonance approximation, $E(\vec{r},t) = \tilde{E}(\vec{r},t)\exp(i\omega(z/c-t)) + C.C.$ with the slowly varying complex amplitude $\tilde{E}(\vec{r},t)$. Using paraxial approximation one can obtain the following expression for $\tilde{E}(\vec{r},t)$:

$$\begin{aligned}\tilde{E}(z,\vec{r}_\perp,t) &= i\frac{\omega}{c^2}\int_0^z \frac{dz'}{z-z'} \\ &\times \int d\vec{r}_\perp \tilde{j}_1(z',\vec{r}'_\perp, t-\frac{z-z'}{c}) \\ &\times \exp\left[\frac{i\omega \mid \vec{r}_\perp - \vec{r}'_\perp \mid^2}{2c(z-z')}\right] . \end{aligned} \quad (1)$$

Simulation code is organized as follows. We divide the electron beam in a large number of elementary volumes. The longitudinal size of each volume is equal (or multiple) to the radiation wavelength. Also, the electron beam is divided into a large number of divisions in the transverse direction. The FEL equations for the particle motion in each elementary volume are solved at each integration step. Then the radiation fields are calculated for each elementary volume using integral solution (1). At the next integration step these fields are substituted into the FEL equations, etc. As a result, one can trace the evolution of the radiation field and the particle distribution when the electron beam passes the undulator. One can obtain from the integrals (1) that the radiation field at each point is defined only by the sources located closer than the slippage distance and there is not necessary to keep in the memory all the current sources. The procedure of the simulations begins from the tail slice of the electron bunch and the procedure of integration is performed over the whole undulator length. Then the equation of motion for the second slice are integrated taking into account the radiation field from the first slice, etc. As a result, the self-consistent FEL equations can be integrated for the electron bunch of any length. The memory requirements for the code are rather moderate. Our experience shows that a few tens of megabytes is sufficient to simulate with sufficient accuracy the most number of practical devices.

The code is realized in two versions: linear and nonlinear. The linear simulation code is based on solution of the kinetic equation describing evolution of the distribution function of the electron beam, and the nonlinear simulation code uses traditional technique of macroparticles for the simulation of the distribution function of the electron beam.

3. Self-consistent equations

To be specific, in this section we present explicit formulae implemented in the code for the simulation of the FEL amplifier with an axially symmetric electron beam. The transverse distribution of the beam current density is assumed to be the Gaussian, $j(r,z) = I(z)\exp(-r^2/2\sigma_r^2)/\sqrt{(2\pi\sigma_r^2)}$ with $\sigma_r = \sqrt{\epsilon_n\beta/\gamma}$ where ϵ_n is rms normalized emittance, β is focusing beta function and $\gamma = \mathcal{E}_0/m_ec^2$ is relativistic factor. The electron beam is divided into $L = l_b/k\lambda$ slices in the longitudinal direction (k is integer number), in M slices over azimuthal angle ϕ, and in N divisions in the radial direction (we use the polar coordinate system (r, ϕ, z) here). As a result, we have $L \times M \times N$ elementary volumes. The self-consistent equations for the linear simulation code are as follows [1, 3]:

$$\begin{aligned}&\frac{d^2b_1}{d\hat{z}^2} + 2i\hat{C}\frac{db_1}{d\hat{z}} + \left[\hat{\Lambda}_p^2\alpha(\hat{r},\hat{z},t) - \hat{C}^2\right]b_1 \\ &= \sum_n \exp(in\phi)U_r^{(n)}(\hat{r},\hat{z},t) , \end{aligned} \quad (2)$$

where $b_1(\hat{r},\hat{z},\phi,t)$ is the beam bunching in the elementary volume, $\alpha(\hat{r},\hat{z},t) = I(\hat{z},t)\exp(-\hat{r}^2)/I_{max}$ and $U_r^{(n)}(\hat{z},\hat{r})$ is the n-th azimuthal harmonic of the effective potential of interaction of the particle with the electromagnetic radiation:

$$\begin{aligned}U_r^{(n)} &= U_{ext}^{(n)}(\hat{z},\hat{r},t) \\ &+ e^{in\pi/2}\int_0^{\hat{z}} \frac{d\hat{z}'}{\hat{z}-\hat{z}'}\int \hat{r}'d\hat{r}'\alpha(\hat{r}',\hat{z}',t-(z-z')/c) \\ &\times b_1^{(n)}(\hat{z}',\hat{r}',t-(z-z')/c)) \\ &\times J_n\left(\frac{B\hat{r}\hat{r}'}{\hat{z}-\hat{z}'}\right)\exp\left\{\frac{iB(\hat{r}^2+\hat{r}'^2)}{2(\hat{z}-\hat{z}')}\right\} . \end{aligned} \quad (3)$$

Here term $U_{ext}^{(n)}(\hat{z},\hat{r})$ corresponds to the external electromagnetic field, $b_1^{(n)}(\hat{r},\hat{z},t)$ are azimuthal harmonics of the beam bunching calculated using the values of $b_1(\hat{r},\hat{z},\phi,t)$ and J_n are the Bessel functions.

When writing down the normalized equations we used the following notations. The transverse coordinate is normalized as $\hat{r} = r/\sqrt{2\sigma_r^2}$. The corresponding reduced variables are as follows: $\hat{z} = \Gamma z$ is reduced longitudinal coordinate, $\hat{C} = (2\pi/\lambda_w - \omega/(2c\gamma_z^2))/\Gamma$ is the detuning parameter, $\hat{\Lambda}_p^2 = \Lambda_p^2/\Gamma^2 = 4c^2(\theta_s\sigma_r\omega A_{JJ})^{-2}$

is the space parameter, $B = 2\Gamma\sigma_r^2\omega/c$ is the diffraction parameter, and the gain parameter Γ is

$$\Gamma = \left[I_{\max} A_{JJ}^2 \omega^2 \theta_s^2/(2I_A c^2 \gamma_z^2 \gamma)\right]^{1/2} \quad , \qquad (4)$$

where $\omega = 2\pi c/\lambda$ is the frequency of the radiation field and $I_A = m_e c^3/e$. Undulator is assumed to be planar with amplitude of the magnetic field H_w and period λ_w. The undulator parameter K, the angle of electron oscillations θ_s, the longitudinal relativistic factor γ_z and the factor A_{JJ} are defined as follows: $K = eH_w\lambda_w/2\pi m_e c^2$, $\theta_s = K/\gamma$, $\gamma_z^2 = \gamma^2/(1+K^2/2)$ and $A_{JJ} = J_0(K^2/(4+2K^2)) - J_1(K^2/(4+2K^2))$, where J_0 and J_1 are the Bessel functions.

In the nonlinear simulation code the electron beam distribution function is simulated with N_p macroparticles in each elementary volume. The equations of motions for the macroparticle written down in the "energy-phase" variables are as follows (for the low efficiency approximation):

$$\begin{aligned} \frac{d\hat{P}}{d\hat{z}} &= \mathrm{Re}\left[2ie^{i\psi}\sum_n \exp(in\phi)U_r^{(n)}(\hat{r},\hat{z})\right] + U_c \\ \frac{d\psi}{d\hat{z}} &= \hat{C} + \hat{P} \ , \end{aligned} \qquad (5)$$

where $\hat{P} = (\mathcal{E} - \mathcal{E}_0)/\rho\mathcal{E}_0$ is the reduced energy deviation, ψ is the phase of the macroparticle within the longitudinal slice and $\rho = c\gamma_z^2\Gamma/\omega$ is the efficiency parameter. Algorithm for the calculation of the space charge contribution, U_c, can be found in ref. [3]. Complex amplitude of the beam bunching is calculated by the averaging of the macroparticle ensemble in the elementary volume, $b_1 = \langle\exp(i\psi_k)\rangle$, and is used for the calculations of the azimuthal harmonics of $b_1^{(n)}$. Equations (5) can be simply extended to the case of a high efficiency approximation and undulator tapering [3, 4]. Complication for the case of the betatron oscillations and the undulator field errors to be taken into account is also straightforward [5].

Analysis of the integrals (3) shows that at chosen radial mesh and at a fixed integration step Δz, calculations can be simplified significantly, since there is finite set of the combination of the values $z - z'$, r and r'. The integrals over Δz for each of the combinations are calculated only once for "unit" source term b_1. Then these data are transferred into the simulation code solving the self-consistent equations. Such a trick allows one to reduce drastically the required CPU time for the field calculations, since at each integration step the computer calculates simple sums weighted by the current sources.

The procedure for the solution of the self-consistent equations (5) has been described in the previous section. The accuracy of the calculations is controlled by means of changing the number of the axial, radial and azimuthal divisions, and the number of the azimuthal modes for the calculations of the radiation field. The criterium is that the final result is independent on the details of the simulations. Figures 1 and 2 present the test results of the simulation code operating in a high gain, steady-state limit. It is seen that there is a good agreement between analytical [1] and simulation results. The relative accuracy for the calculation of the radiation field and the gain is about 0.1 %.

At the exit the simulation code produces the matrixes for the field values in the Fresnel diffraction zone. Then the post-processor programs are used to

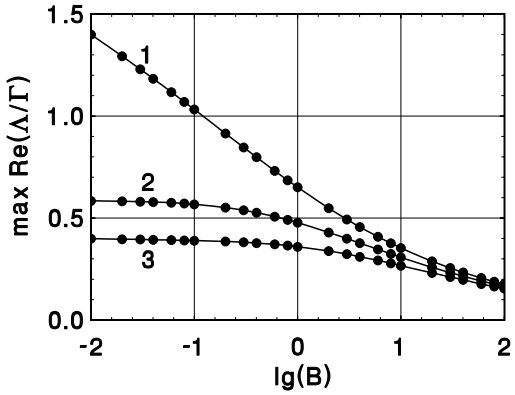

Fig. 1. The dependence of the maximal reduced field gain $\max \mathrm{Re}(\Lambda/\Gamma)$ on the diffraction parameter B. Here $\hat{\Lambda}_p^2 = 0$, $\hat{\Lambda}_T^2 = 0$. Curve (1): TEM_{00} mode, curve (2): TEM_{10} mode and curve (3): TEM_{01} mode. Solid curves are analytical results and the circles are the results of the numerical simulation code.

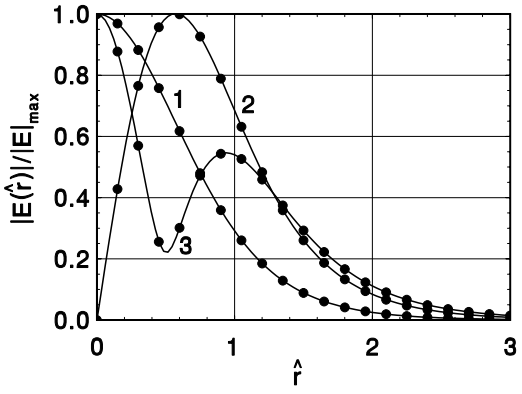

Fig. 2. Transverse distribution of the radiation field for TEM_{00}, TEM_{10} and TEM_{01}. Here $B = 10$, $\hat{\Lambda}_p^2 = 0$ and $\hat{\Lambda}_T^2 = 0$. Curve (1): TEM_{00}, curve (2): TEM_{10} mode and curve (3): TEM_{01} mode. Solid curves are analytical results and the circles are the results of the numerical simulation code.

extract additional information for the field distribution in the far diffraction zone, for the spectrum, for the time, space and spectral correlation functions, and for the probability distributions of the radiation power and the radiation energy (see, e.g. ref [6]).

4. Initial conditions for the start-up from noise

The initial shot noise in the electron beam is simulated according to the algorithm presented in the paper [6]. The number of particles per elementary volume N_v is large, so the bunching in each box is the sum of large number of random phasors with fixed amplitudes and uniformly distributed on $(0, 2\pi)$ phases. Using the central limit theorem, we can conclude that phases of bunching parameters are distributed also uniformly and squared modules of amplitudes, $\mid b_1 \mid^2$, are distributed in accordance with the negative exponential distribution:

$$p(\mid b_1 \mid^2) = \frac{1}{<\mid b_1 \mid^2>} \exp\left(-\frac{\mid b_1 \mid^2}{<\mid b_1 \mid^2>}\right) , \qquad (6)$$

where $<\mid b_1 \mid^2> = 1/N_v$. The distribution of the modules, $\mid b_1 \mid$, is the Rayleigh probability density function. So, we use the negative exponential random generator setting $1/N_v$ as mean value to extract the values of $\mid b_1 \mid^2$ for each box and then we extract the square root to find the values of $\mid b_1 \mid$. The phases of b_1 are produced by random generator of uniform distribution from 0 to 2π. These values are directly used as input parameters for the linear simulation code. In the nonlinear simulation code the macroparticles are distributed in such a way that the resulting bunching corresponds to the target value of b_1 in each elementary volume.

5. Conclusion

In conclusion we should notice that the speed of calculations is an essential parameter for the FEL code calculating the start-up from noise. The reason for this is that the most important characteristics of the SASE FEL (the spectrum, time, space and spectral correlation functions and the probability distributions of the radiation power and energy) can be calculated only with statistical analysis of a large number of simulation runs [6]. For instance, the number of the simulation runs required for the calculation of the probability distribution of the radiation energy in the pulse is about several thousands. The presented code allows one to calculate all the above mentioned statistical parameters of the SASE FEL within reasonable time. For instance, typical simulation run with the linear simulation code for the parameters of UCLA/LANL/RRCKI/SLAC SASE FEL [7] takes about one minute at VAX processor [8] This is about two orders of magnitude less than the time required by another time-dependent codes (such as GINGER or GENESIS) to obtain the same physical result [9, 10].

Acknowledgments

We are grateful to B. Faatz, J. Feldhaus, G. Materlik, J. Pflüger, S. Reiche, J. Roßbach and J.R. Schneider for many useful discussions.

References

[1] E.L. Saldin, E.A. Schneidmiller and M.V. Yurkov, Opt. Commun. **97**(1993)272.

[2] E.L. Saldin, E.A. Schneidmiller and M.V. Yurkov, Opt. Commun. **95**(1993)141.

[3] E.L. Saldin, E.A. Schneidmiller and M.V. Yurkov, Phys. Rep. **260**(1995)187.

[4] C. Pagani, E.L. Saldin, E.A. Schneidmiller and M.V. Yurkov, "Design Considerations and Analysis of Potential Applications of a High Power Ultraviolet FEL at the TESLA Test Facility at DESY", Nuclear Instruments and Methods A, in press.

[5] T.M. Tran and J.S. Wurtele, Comput. Phys. Commun. **54**(1989)263.

[6] E.L. Saldin, E.A. Schneidmiller and M.V. Yurkov, Opt. Commun. **148**(1998)383.

[7] M. Hogan, C. Pellegrini, J. Rosenzweig, A. Anderson, P. Frigola, A. Tremaine, C. Fortgang, D. Nguyen, R. Sheffield, J. Kinross-Wright, A. Varfolomeev, A.A. Varfolomeev, S. Tolmachev, R. Carr, "Measurement of Gain Larger Than 10^5 at 12 μm in a SASE FEL", submitted to Physical Review Letters.

[8] E.L. Saldin, E.A. Schneidmiller and M.V. Yurkov, "Numerical Simulations of the UCLA/LANL/RRCKI/SLAC Experiment on a High Gain SASE FEL", Presentation at the 20th FEL Conference, Williamsburg, 1998.

[9] P. Pierini and W. Fawley, Nucl. Instrum. and Methods **A375**(1996)332.

[10] S. Reiche, "GENESIS 1.3- A Fully 3D Time Dependent FEL Simulation Code", Presentation at the 20th FEL Conference, Williamsburg, 1998.

Growth of the Energy Spread Due to the Radiative Interaction in a Short Electron Bunch Moving in an Undulator

E.L. Saldin[a], E.A. Schneidmiller[a], M.V. Yurkov[b]

[a] *Automatic Systems Corporation, 443050 Samara, Russia*

[b] *Joint Institute for Nuclear Research, Dubna, 141980 Moscow Region, Russia*

Abstract

This paper presents investigations of the longitudinal radiative force in an electron bunch moving in an undulator (wiggler). Analytical solution is obtained for a Gaussian longitudinal bunch profile. Radiative interaction of the particles in an intensive microbunch induces a correlated energy spread in the electron beam. Numerical estimations presented in the paper show that this effect can be important for free electron lasers.

1. Introduction

The theory of the radiative interaction of the electrons in an intensive microbunch traversing curved trajectory is intensively developed nowadays. This is explained by the practical importance of the radiative effects for the beam dynamics in linear colliders and short-wavelength free electron lasers. When intensive electron bunch passes bending magnets, bunch compressors, wigglers etc, the radiative interaction induces the energy spread in the electron beam and can lead to the transverse emittance dilution in dispersive regions.

In this paper we present the results of analytical calculation of the radiative interaction of particles in a bunch with the line-charge distribution moving in an undulator (a wiggler) [1]. The transient effects (when the bunch enters and leaves the undulator) are withdrawn from the consideration and the shielding effects (influence of a vacuum chamber on the radiative process) are neglected. Practical application of the obtained results is illustrated with the numerical examples for the proposed SASE FELs. Also, the testing of the numerical simulation codes would be difficult without rigorous analytical results.

2. General solution for a bunch moving in an undulator

Let us consider the electron bunch with a linear density of particles $\lambda(s)$ moving along the z direction in the undulator with with magnetic field

$$H_x = H_w \cos(k_w z) \ .$$

The transverse and the longitudinal velocities of an electron can be approximated by

$$\beta_y = \frac{K}{\gamma}\sin(k_w z), \qquad \beta_z = \beta - \frac{K^2}{2\gamma^2}\sin^2(k_w z) \ ,$$

where $K = eH_w/k_w mc^2$ is the undulator parameter, $\gamma = \mathcal{E}/mc^2$ is relativistic factor, $(1 + K^2/2)/\gamma^2 \ll 1$ and $\beta \simeq 1 - 1/2\gamma^2$. Transverse coordinate of the electron oscillates as

$$y = -\frac{K}{\gamma k_w}\cos(k_w z) \ .$$

The bunch length is assumed to be much shorter than the undulator period $2\pi/k_w$. We calculate the longitudinal (along the particle's velocity) radiative force assuming the motion of the particles to be given. Only the interaction connected with the curvature is considered and we omit the trivial longitudinal space-charge forces in a bunch moving on a straight line, since they can be calculated separately. The calculations are based on the general algorithm for an arbitrary small-angle trajectory described in ref. [1]. Leaving the details of the calculations, we present the final result for the rate of the energy change as a function of the positions of the electron in the bunch and in the undulator, s and z, respectively [1]:

$$\frac{d\mathcal{E}}{cdt} = e^2 k_w \int_{-\infty}^{s} ds' D(\hat{s}-\hat{s}', K, \hat{z}) \frac{d\lambda(s')}{ds'} \ , \qquad (1)$$

where

$$D(\hat{s}, K, \hat{z}) = \frac{1}{\hat{s}} - 2\ \frac{\Delta - K^2 B(\Delta, \hat{z})}{\Delta^2 + K^2 B^2(\Delta, \hat{z})} \times [\sin\Delta \cos\hat{z} + (1-\cos\Delta)\sin\hat{z}] \ , \qquad (2)$$

$$B(\Delta, \hat{z}) = (1 - \cos\Delta - \Delta\sin\Delta)\cos\hat{z} + (\Delta\cos\Delta - \sin\Delta)\sin\hat{z} \ , \qquad (3)$$

and Δ is the solution of the transcendental equation:

$$\hat{s} = \frac{\Delta}{2}\left(1 + \frac{K^2}{2}\right) + \frac{K^2}{4\Delta}\{[2(1-\cos\Delta) - \Delta\sin\Delta] \times (\cos\Delta\cos 2\hat{z} + \sin\Delta\sin 2\hat{z}) - 2(1-\cos\Delta)\} \ . \qquad (4)$$

Here the following reduced variables are introduced: $\hat{s} = \gamma^2 k_w s$ and $\hat{z} = k_w z$.

It follows from the geometry of the problem and from eqs. (2) – (4) that function D is periodical in z. with the period equal to the half of the undulator period π/k_w (or, to π in terms of the normalized position $\hat{z}$). In the following we will study the rate of the energy change averaged over the z coordinate:

$$\frac{d\bar{\mathcal{E}}}{cdt} = e^2 k_w \int_{-\infty}^{s} ds' \bar{D}(\hat{s}-\hat{s}', K) \frac{d\lambda(s')}{ds'} \ , \qquad (5)$$

where

$$\bar{D}(\hat{s}, K) = \frac{1}{\pi}\int_0^{\pi} d\hat{z} D(\hat{s}, K, \hat{z}) \ . \qquad (6)$$

In the case of small values of the undulator parameter, $K \ll 1$, the function $\bar{D}(\hat{s}, K)$ takes the simple form:

$$\bar{D}(\hat{s}, K) = -K^2\left(\frac{\sin^2\hat{s}}{\hat{s}} + \frac{\sin 2\hat{s}}{2\hat{s}^2} - \frac{\sin^2\hat{s}}{\hat{s}^3}\right) \ . \qquad (7)$$

3. Averaged solution for a Gaussian bunch

In this section we consider a bunch with a Gaussian distribution of linear density:

$$\lambda(s) = \frac{N}{\sqrt{2\pi}\sigma}\ \exp\left[-\frac{s^2}{2\sigma^2}\right] \ . \qquad (8)$$

The averaged solution for the Gaussian bunch can be written in the form:

$$\frac{d\bar{\mathcal{E}}}{cdt} = \frac{e^2 N K^2}{\sqrt{2\pi}\sigma^2\gamma^2}\bar{G}(p, K, x) \ , \qquad (9)$$

where $x = s/\sigma$ and p is the bunch length parameter:

$$p = \frac{\gamma^2 k_w \sigma}{1 + K^2/2} \ .$$

In the general case function $\bar{G}$ should be calculated by means of numerical integration of eq. (5). Nevertheless, in some region of parameters it can be expressed analytically. Let us study practically important case of a long bunch, $p \gg 1$. First, we consider the case of small K. Under these conditions function $\bar{G}$ can be calculated analytically using eqs. (5) and (7):

$$\bar{G}(p, x) = \frac{x}{2}\exp\left(-\frac{x^2}{2}\right)\ln p + F(x) \ . \qquad (10)$$

Here parameter p is reduced to $p \simeq \gamma^2 k_w \sigma$, and function $F(x)$ has the form:

$$F(x) = \frac{1}{4}(C + 3\ln 2 - 2)x\exp\left(-\frac{x^2}{2}\right) - \sqrt{\frac{\pi}{8}}\left[1 + \mathrm{erf}\left(\frac{\mathrm{x}}{\sqrt{2}}\right) - \mathrm{x}\exp\left(-\frac{\mathrm{x}^2}{2}\right) \times \int_0^x dx' \exp\left(\frac{(x')^2}{2}\right)\left(1 + \mathrm{erf}\left(\frac{\mathrm{x}'}{\sqrt{2}}\right)\right)\right] \ , \qquad (11)$$

where $C = 0.577...$ is the Euler's constant and $\mathrm{erf}(...)$ is the error function [2]. The plot of function $F(x)$ is presented in Fig. 1. Figure 2 presents the plots of function $\bar{G}$ calculated at different values of parameter p.

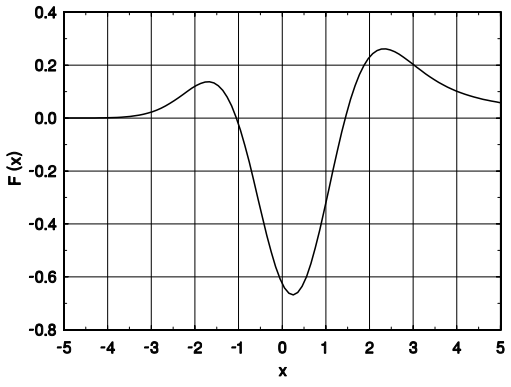

Fig. 1. Function $F(x)$ given by eq. (11).

In the case of an arbitrary value of the undulator parameter K, it is difficult to find explicit analytical solution. Nevertheless, using the results of numerical

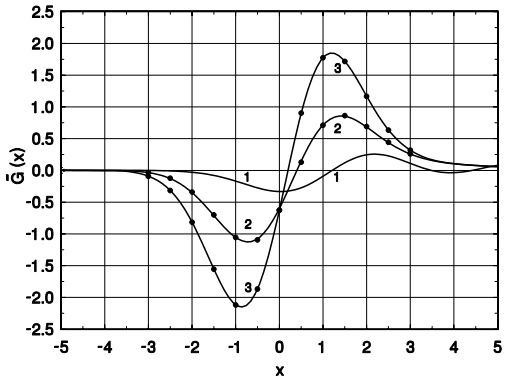

Fig. 2. Function $\bar{G}$ for small value of the undulator parameter K and different values of the bunch length parameter p. Curve (1): $p = 1$, curve (2): $p = 30$, and curve (3): $p = 1000$. The curves are the results of numerical integration of eq. (5) and the circles are calculated with the help of analytical formula (10) for large values of parameter p.

integration of eq. (5), we can write function $\bar{G}$ in the following form ($p \gg 1$):

$$\bar{G}(p, K, x) = \frac{x}{2} \exp\left(-\frac{x^2}{2}\right) [\ln p + g(K)] + F(x) \ , \tag{12}$$

where function $g(K)$ changes from 0 to 1 when K changes from small to large values. The plot of this function is presented in Fig. 3.

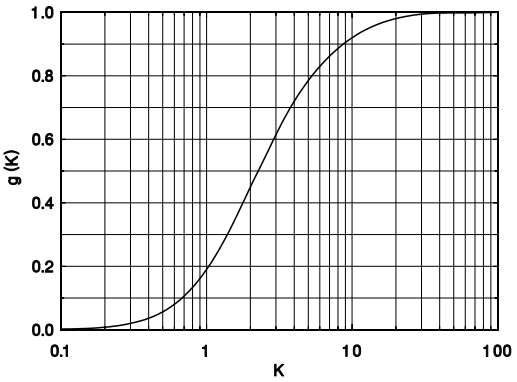

Fig. 3. Function $g(K)$ entering eq. (12).

In conclusion to this section we present the formula for the induced correlated energy spread in the Gaussian bunch due to the radiative interaction. Using expression (12) we write down this formula in the form convenient for practical calculations ($p \gg 1$):

$$\sigma_\gamma = 0.219 \frac{I K^2 L_w}{I_A \sigma \gamma^2} \times$$

$$\sqrt{[\ln p + g(K)]^2 + 0.933[\ln p + g(K)] - 0.786} \ , \tag{13}$$

where $I = Nec/\sqrt{2\pi}\sigma$ is the peak current, $I_A = 17$ kA is Alfven current, L_w is the undulator length and

$$mc^2 \sigma_\gamma = \sqrt{\langle \bar{\mathcal{E}}^2 \rangle - \langle \bar{\mathcal{E}} \rangle^2} \ .$$

4. Discussion

Let us perform estimations of the applicability region of the obtained results for the practically important case of a long bunch, $\sigma \gg (1 + K^2/2)/\gamma^2 k_w$. First, we consider the transient effects. When the behaviour of the radiative forces after the bunch leaves the undulator is not important from practical point of view (which is true for FELs), only the entrance transient effect is of interest. In this case we can write down the following limitation on the undulator (wiggler) length L_w, allowing us to neglect transient effects:

$$L_w \gg \sigma \gamma_z^2 \ , \tag{14}$$

where $\sigma\gamma_z^2 = \sigma\gamma^2/(1 + K^2/2)$ is typical formation length of the radiation.

Second, we estimate the region of parameters where we can neglect the influence of the bunch transverse size and of the vacuum pipe. It follows from simple geometrical consideration that a characteristic measure distinguishing these effects is the mean geometric value of the bunch length and the formation length of the radiation. Thus, we can roughly estimate the region where the considered effects can be neglected:

$$\sigma_\perp \ll \sigma\gamma_z \ll b \ . \tag{15}$$

Here $\sigma_\perp$ and b are transverse dimensions of the bunch and of the vacuum chamber, respectively.

When the above mentioned limitations are not satisfied, the considered effects become to be important leading to suppression of the radiative interaction. In other words, the model considered in this paper describes the worst-case approximation, which makes it useful for quick estimations of the radiative interaction effects. Also, analytical results presented in the paper can serve as primary standards for testing numerical simulation codes.

In conclusion to this paper let us illustrate practical application of the obtained results with two numerical examples. The first one is the 6 nm SASE FEL being under construction at the TESLA Test Facility at DESY [3]. Parameters of the project are: the energy is 1 GeV, the rms bunch length is 50 μm, the peak current is 2.5 kA, the undulator period is 2.73 cm, K is 1.27 and the undulator length is 27 m. Substituting these values into formula (13), we obtain that the induced correlated energy spread is equal to

$\sigma_\gamma/\gamma = 4 \times 10^{-5}$ which is negligible. Besides, condition (14) and the condition (15) for the shielding are not satisfied, since the diameter of vacuum chamber is equal to 1 cm. This will lead to further reduction of the effect. It should be noticed that such a situation is typical for the projects of VUV and X-ray FELs.

The second example is the proposal by the Duke university [4] to construct 1.4 μm SASE FEL using the PALADIN wiggler. The energy is 200 MeV, the rms bunch length is 50 μm, the bunch radius is 0.125 cm, the peak current is 2.5 kA, the wiggler period is 8 cm, K is 3 and the wiggler length is 15 m. Assuming the size of the vacuum chamber to be about 2 cm, we obtain that conditions (14) and (15) are met and our simple model provides correct estimation of the effect. According to formula (13), we obtain $\sigma_\gamma/\gamma = 8.4\times10^{-3}$. Effective operation of the free electron laser requires $\sigma_\gamma/\gamma \ll \rho$, where ρ is the FEL parameter [5]. For the Duke SASE FEL $\rho = 4.8 \times 10^{-3}$, and the latter condition is strongly violated. Besides, the SASE coherence length [6] is of the order of the bunch length. Thus, the large energy spread will be induced within the coherence length and the FEL process will be destroyed.

Acknowledgments

We wish to thank R. Brinkmann, C. Bohn, Ya. Derbenev, M. Dohlus, P. Emma, D. Jaroszynski, J. Krzywinski, R. Li, T. Limberg, J. Rossbach and V. Shiltsev for useful discussions on the radiative interaction effects.

References

[1] E.L. Saldin, E.A. Schneidmiller, and M.V. Yurkov, "Radiative interaction of electrons in a bunch moving in an undulator", DESY Print, TESLA-FEL 97-08, Hamburg(1997).

[2] M. Abramowitz and I.A. Stegun, Handbook of Mathematical Functions, (National Bureau of Standards, 1964).

[3] J. Rossbach, Nucl. Instr. and Methods **A375**(1996)269.

[4] P.G. O'Shea, C.P. Neumann, J.M.J. Madey, and H.P. Freund, Nucl. Instr. and Methods **A393**(1997)129.

[5] R. Bonifacio, C. Pellegrini and L. Narducci, Opt. Commun. **50**(1984)373.

[6] E.L. Saldin, E.A. Schneidmiller and M.V. Yurkov, Opt. Commun. **148**(1998)383.

Numerical Simulations of the UCLA/LANL/RRCKI/SLAC Experiment on a High Gain SASE FEL

E.L. Saldin[a], E.A. Schneidmiller[a], M.V. Yurkov[b]

[a] *Automatic Systems Corporation, 443050 Samara, Russia*

[b] *Joint Institute for Nuclear Research, Dubna, 141980 Moscow Region, Russia*

Abstract

In this paper we present theoretical analysis of a recent SASE FEL experiment performed by UCLA/LANL/RRCKI/SLAC team reporting on a high power gain of about 10^5 at the wavelength of 12 μm The region of physical parameters of this experiment (as well as of future X-ray FELs) does not allow to apply available analytical techniques for quantitative description of the obtained results. The analysis presented in this paper is based on the results produced by a three-dimensional, time-dependent FEL simulation code FAST. It is shown that within the limit of accuracy of the experiment obtained data fully agree with the results of numerical simulations.

1. Introduction

Recently it has been reported on an operation of a high gain FEL amplifier starting from noise [1] (see Table 1). The power gain of larger than 10^5 has been obtained. Parameters of the output radiation have been measured with a high accuracy. In particular, it has been demonstrated that the fluctuations of the energy in the radiation pulse follows the gamma distribution predicted in ref. [2, 3]. Thorough analysis shows that despite this experiment has been performed at a relatively long wavelength, the physical processes in this SASE FEL are similar to those expected to occur in a short wavelength SASE FEL. This is connected with the fact that the aperture of the vacuum chamber is significantly larger than the transverse size of the beam radiation mode. As a result, the waveguide effects do not influence the amplification process. Also, the effects of coherent synchrotron radiation are not important at the chosen parameters of the experiment. Helpful factor simplifying analysis of this experiment consists in careful choice of experimental conditions. Namely, undulator field has been tuned precisely and distortions of the electron beam trajectory are significantly less than typical transverse size of the beam radiation mode. There is also significant safety margin with respect to the energy spread and the emiitance of the electron beam.

Table 1. Parameters of the UCLA/LANL SASE FEL [1]

Electron beam	
Energy [MeV]	18
Charge per micropulse [nC]	0.3 – 2.2
Transverse spot size (σ) [μm]	115 – 145
Energy spread (rms) [%]	~ 0.3
Pulse length (FWHM) [ps]	7 – 13
Peak current [A]	40 – 170
Undulator	
Period [cm]	2.05
Number of periods	98
Undulator parameter K	1
Betatron wavelength [m]	1.2
FEL	
Radiation wavelength [μm]	12
Power gain length (at 2.2 nC) [cm]	~ 14

In this paper we perform theoretical analysis of the high gain SASE FEL experiment [1]. The analysis is based on the results produced by a three-dimensional, time-dependent FEL simulation code FAST [4]. Parameters of the electron beam and of the undulator [1] have been introduced "as is" as the input parameters for the numerical simulation code. It is shown that the obtained experimental results are in good agreement with the results of numerical calculations. Statisti-

cal simulations of the energy fluctuations in the radiation pulse performed over several thousands shots give the result identical to the experimental one. Namely, fluctuations of the energy in the radiation pulse follow gamma distribution with the value of parameter $M \simeq 8$.

2. Region of physical parameters

We begin our analysis within the framework of the steady-state approximation in order to estimate the power of different physical effects influencing the operation of the FEL amplifier. Numerical solution of the corresponding eigenvalue equation [5, 6, 7] shows that the main physical effects defining the operation of the UCLA/LANL SASE FEL are the diffraction effects and the space charge effects. It is seen from the plot in Fig. 1 that the field gain length should be about 30 cm. Also, analysis of the imaginary part of the eigenvalue shows that the slippage effect will be suppressed by a factor of four with respect to kinematic slippage due to the fact that the group velocity of the amplified wave, $\partial\omega/\partial k$, is less than the velocity of light c.

3. Numerical analysis of the experiment

Numerical simulations have been performed with three-dimensional, time-dependent FEL simulation code FAST [4]. The equations of motion (kinetic equation or equations for macroparticle motion) and Maxwell's equations are solved simultaneously taking into account the slippage effect. Radiation fields are calculated using integral solution of Maxwell's equations. The code allows one to simulate the radiation from the electron bunch of any transverse and longitudinal bunch shape; to simulate simultaneously external seed with superimposed shot noise in the electron beam; to take into account energy spread in the electron beam and the space charge fields; and to simulate high-gain, high-efficiency FEL amplifier with tapered undulator. The code is extremely fast thus allowing to perform precise statistical calculations.

To calculate averaged characteristics of the FEL amplifier we performed several thousands statistically independent runs. Input data for the numerical simulation code are the value of the undulator period and the peak field, the value of the bunch charge, the value of the bunch length and the bunch radius. When performing simulations we used two models of the axial profile of the bunch current, a gaussian one

$$I(z) = \frac{Qc}{\sqrt{2\pi}\sigma_z} \exp[-\frac{z^2}{2\sigma_z^2}] ,$$

with $\sigma_z = \sigma_z^{\rm HWHM}/\sqrt{2\ln 2}$, and a parabolic one:

$$I(z) = \frac{3Qc}{4\sigma_z}[1 - \frac{z^2}{\sigma_z^2}] , \qquad |z| < \sigma_z ,$$

with $\sigma_z = \sqrt{2}\sigma_z^{\rm HWHM}$. Transverse distribution of the beam current density assumed to be gaussian:

$$j(z,r) = \frac{I(z)}{2\pi\sigma_r^2} \exp[-\frac{r^2}{2\sigma_r^2}] ,$$

with $\sigma_r = \sigma_r^{\rm HWHM}/\sqrt{2\ln 2}$. HWHM values are defined by fitting formulae presented in ref. [1]: $\sigma_{z,r}^{\rm HWHM} = \sqrt{a^2 + (bQ)^2}$. Parameters for the spot size are $a = 120$ μm, $b = 38$ μm/nC, and for the pulse length $a = 3$ ps, $b = 2.2$ ps/nC.

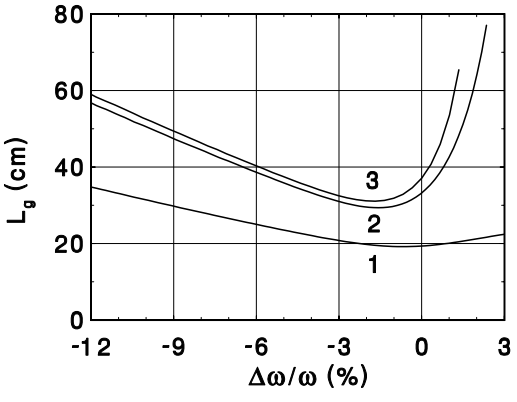

Fig. 1. The field gain length versus the frequency deviation from the resonance value. Calculations have been performed in the steady-state approximation. Curve 1 is calculated with the only diffraction effects taken into account, curve 2 includes also the space charge effects, and curve 3 is calculated taking into account all the effects (diffraction, space charge and energy spread).

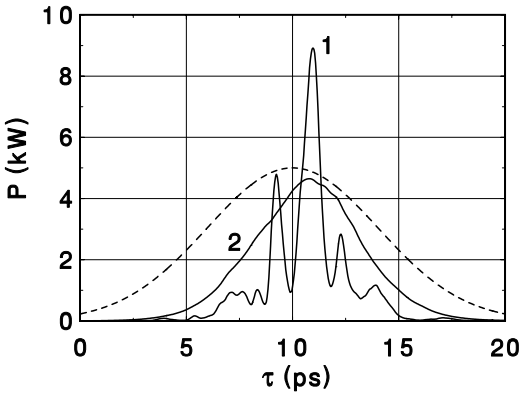

Fig. 2. Typical time structure of the radiation pulse at the undulator exit (curve 1) and time structure of the radiation pulse averaged over 1000 statistically independent runs (curve 2). Dashed line presents axial profile of the beam current. Charge in the electron bunch is 2.2 nC.

In Fig. 2 we present typical time structure of the radiation pulse at the undulator exit at the value of the bunch charge of 2.2 nC. Averaging over one thousand of independent shots gives the value of the averaged radiation pulse shape (curve 2 in Fig. 2). Analysis of the latter plot allows one to obtain the value of the "effective" shot noise power at the undulator entrance to be used in the steady-state codes for obtaining approximate value of the average output power [8, 3]. The value of the "effective" power of shot noise is of about 20 mW in the case under study. It is seen also from Fig. 2 that the slippage of the radiation with respect to the electron bunch is significantly smaller than kinematic one. This is connected with the fact that the group velocity of the spikes, $\partial\omega/\partial k$, is less than the velocity of light c as it has been mentioned in section 2.

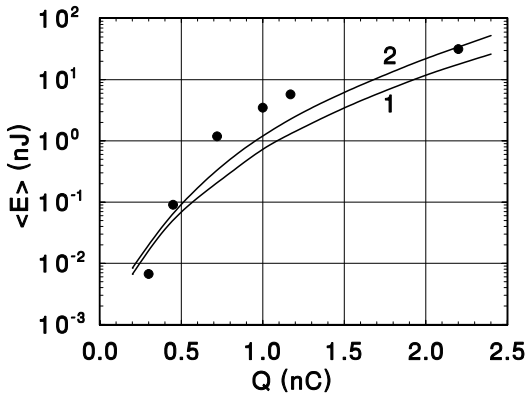

Fig. 3. Dependence of the averaged energy in the radiation pulse versus the bunch charge. Curves 1 and 2 correspond to the gaussian and the parabolic axial beam profiles. The circles are experimental results [1].

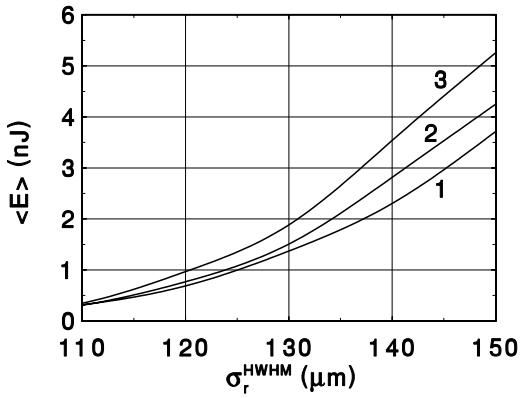

Fig. 4. Dependence of the averaged energy in the radiation pulse on the transverse bunch size. Curves 1, 2 and 3 correspond to the values of the longitudinal HWHM bunch size $\sigma_z^{\rm HWHM}$ of 3.9 ps, 3.7 ps and 3.5 ps, respectively. The bunch charge is 1 nC.

In Fig. 3 we present comparison of experimental and simulation results for different values of the charge. Fig. 4 presents the dependency of the energy in the radiation pulse on the transverse and longitudinal beam sizes at a fixed value of the bunch charge of 1 nC. It is seen that within uncertainties in measuring these values [1, 9, 10], numerical and experimental results agree rather well. One can also obtain unusual behaviour of the energy in the radiation pulse on the value of the transverse beam size. Namely, the radiation energy is increased at the increase of the transverse beam size. This effect is connected with the fact which we have mentioned in section 2 that UCLA/LANL FEL amplifier operates in the regime of a strong influence of the space charge effects. In the case under study the diffraction parameter B is much less than unity, and increasing of the beam size results only in logarithmic decreasing of the field gain due to diffraction effects [5, 6]. On the other hand, there is strong influence of the space charge fields. Increasing of the transverse beam size leads to quadratic decrease of the space charge parameter which results in the increase of the field gain. In the region of parameters traced in Fig. 4 this effect dominates above the diffraction effects. As a result, the field gain and the energy in the radiation pulse grow with the increase of the transverse size of the electron beam. Calculations show that such a tendency will take place up to the value of diffraction parameter $B \sim 0.3$. Above this pont the space charge effect becomes to be a small perturbation to the FEL process and increase of the transverse beam size will lead to the decrease of the field gain (see, e.g. ref. [11]).

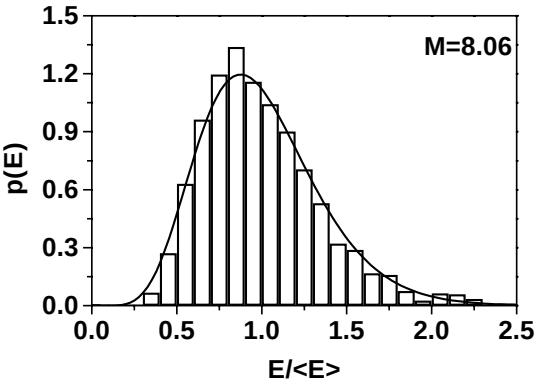

Fig. 5. Probability distribution of the energy in the radiation pulse at the bunch charge of 2.2 nC calculated over 2400 statistically independent runs. Solid curve presents gamma distribution with $M = 8.06$.

So, we see that there is good agreement between measurements of the energy in the radiation pulse and the simulation results. Indeed, in all the region of the charge of the electron beam (see Fig. 3), the relative

difference recalculated in the units of the gain length is less than one power gain length. Taking into account good agreement of the energy in the radiation pulse, we can expect much better agreement with the probability distribution of the energy in the radiation pulse. We performed the corresponding simulations at the value of the bunch charge of 2.2 nC. Simulations show that the probability distribution of the energy in the radiation pulse is quite close to the gamma distribution

$$p(E) = \frac{M^M}{\Gamma(M)} \left(\frac{E}{< E >}\right)^{M-1} \frac{1}{< E >} \exp\left(-M \frac{E}{< E >}\right) ,$$

where $\Gamma(M)$ is the gamma function of argument M. Parameter of the distribution is equal to $M = 1/\sigma^2$, where $\sigma^2 = \langle E^2 - \langle E \rangle^2 \rangle / \langle E \rangle^2$ is the normalized dispersion of the energy distribution. The first set of runs has been performed at fixed values of the bunch charge, of the transverse beam size and of the longitudinal beam size. Simulations with the gaussian and the parabolic bunch profiles give very close results, namely that $M \simeq 11.5$ and $\sigma \simeq 30$ %. On the other hand, experimental result gives the value of the fluctuations of about $\sigma \simeq 37$ %. Such a visible difference indicates that shot-to-shot fluctuations of the beam parameters contribute to the fluctuations of the radiation energy. To take these fluctuations into account we performed 2400 statistically independent runs. During each run the fluctuations have been introduced in the following limits: ± 0.75 % for the bunch charge, ± 5.5 % for the transverse beam size and ± 6 % for the bunch length [1]. The results of the simulations are shown in Fig. 5. The probability distribution of the radiation energy follows the gamma distribution with $\sigma \simeq 35$ % and $M \simeq 8$. This result is in a good agreement with the experiment.

4. Conclusion

In conclusion we should like to notice that there is no doubt that UCLA/LANL experiment [1] is a proof-of-principle of a high-gain SASE FEL. Despite it has been performed at a relatively long wavelength, the physics of its operation is described with the same equations as future VUV and X-ray SASE FELs. All the simulations presented in this paper have been performed with the simulation code developed for simulation of short-wavelength SASE FELs. It is seen that there is good agreement between theoretical predictions and experimental results, which forms reliable base for future design of short-wavelength SASE FELs.

Acknowledgments

We are extremely grateful to C. Pellegrini and A. Varfolomeev for providing us with experimental results and fruitful discussions. We wish to thank B. Faatz, J. Feldhaus, J. Krzywinski, G. Materlik, T. Möller, C. Pagani, J. Pflüger, S. Reiche, J. Roßbach and J.R. Schneider for many useful discussions.

References

[1] M. Hogan, C. Pellegrini, J. Rosenzweig, A. Anderson, P. Frigola, A. Tremaine, C. Fortgang, D. Nguyen, R. Sheffield, J. Kinross-Wright, A. Varfolomeev, A.A. Varfolomeev, S. Tolmachev, R. Carr, "Measurement of Gain Larger Than 10^5 at 12 μm in a SASE FEL", submitted to Physical Review Letters.

[2] E.L. Saldin, E.A. Schneidmiller and M.V. Yurkov, DESY Print TESLA-FEL 97-02, April, 1997.

[3] E.L. Saldin, E.A. Schneidmiller and M.V. Yurkov, Opt. Commun. **148**(1998)383.

[4] E.L. Saldin, E.A. Schneidmiller and M.V. Yurkov, "FAST: Three dimensional, time-dependent FEL simulation code", presentation at the 20 th FEL Conference.

[5] E.L. Saldin, E.A. Schneidmiller and M.V. Yurkov, Phys. Rep. **260**(1995)187.

[6] E.L. Saldin, E.A. Schneidmiller and M.V. Yurkov, Opt. Commun. **97**(1993)272.

[7] E.L. Saldin, E.A. Schneidmiller and M.V. Yurkov, DESY Print May 1995, TESLA-FEL 95-02, Hamburg, DESY, 1995.

[8] K.J. Kim, Nucl. Instrum. and Methods **A250**(1986)396.

[9] R.L. Sheffield et al., Nucl. Instrum. and Methods **A341**(1994)371.

[10] S.H. Kong et al., Nucl. Instrum. and Methods **A358**(1995)284.

[11] E.L. Saldin, E.A. Schneidmiller and M.V. Yurkov, Proceedings of the Fifth European Particle Accelerator Conference, Vol.1, pp. 471-473 (Institute of Physics Publishing, Bristol, 1996).

Concept of Electron Beam Diagnostic for the VUV SASE FEL at the TESLA Test Facility (TTF FEL) at DESY

G. Schmidt, U. Hahn, J. Pflüger

Deutsches Elektronen-Synchrotron (DESY), Notkestrasse 85, D-22607 Hamburg, Germany

Abstract

The electron beam trajectory inside an undulator with integrated strong focusing quadrupoles is disturbed by any kind of magnetic or alignment errors of the guiding field. The electron and photon beam must overlap over the entire undulator length to achieve an optimum output of the TTF FEL [1]. Therefore it is necessary to measure and correct the electron beam trajectory. The orbit correction in the undulator is based on two principles of orbit measurement. The absolute position of the electron beam inside the undulator can be measured at 4 points of support with calibrated monitors. The second method of measuring the beam trajectory is a beam based alignment algorithm which uses relative orbit changes at 30 distributed beam position monitors along the undulator. A mismatching of the optic at the entrance of the undulator can be seen by measuring the beam size at different locations along the undulator.

1. Introduction

The TTF FEL uses an undulator with integrated strong focusing quadrupoles. The undulator consists of three undulator sections with integrated strong focusing quadrupoles. Each undulator section contains 10 quadrupole magnets building a FODO structure. At the entrance, the exit and in between the undulator sections diagnostic blocks are installed as shown in figure (1). Orbit deviations inside the undulator are introduced by unknown, random dipole kicks, due to the error in the planar undulator structure, and kicks due to misaligned quadrupoles. To correct the errors of the 30 quadrupoles, for each quadropole a steerer and a beam position monitor (BPM) are installed.

The diagnostic inside the undulator is necessary to align the electron beam within 10 μm rms deviation to a straight line. This ensures the overlap of the electron and photon beam over the entire undulator length to keep the gain reduction of the FEL smaller than 15 % in phase 1 of the TTF FEL project [1]. It is foreseen to use the undulator at electron beam energies between 200 and 500 MeV. Due to the fact that the magnet strength is fixed inside the undulator the optical functions inside the undulator change with the beam energy. To

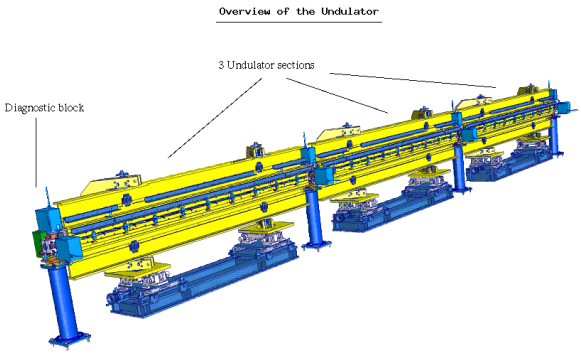

Fig. 1. Three undulator sections with four diagnostic blocks.

get a periodic beta function the optic is adapted to the beam energy at the entrance of the undulator. A mismatching of the optic at the entrance of the undulator can be detected by using four wire scanners along the undulator.

Table 1: TTF FEL Phase 1 in Numbers [1]	
Beam energy	200 to 500 MeV
Normalized emittance	2 πmm mrad
Average beam size inside the Undulator	0.08 mm
Charge per bunch	0.1 to 1 nC
Bunch repetition rate	1 MHz
Macropulse repetition rate	up to 10 Hz
Macropulse length	up to 800 μs
Chamber Diameter inside the Undulator	9.6 mm
Number of undulator sections	3
Undulator gap height	12 mm
Undulator section length	4.5 m
Undulator period length	27.3 mm
Gradient inside the undulator	12.5 T/m
Number of BPM's inside one section	10
Number of diagnostic blocks	4
Number of wire scanners	4 hor. and ver.
Number of cavity monitors	4 hor. and ver.

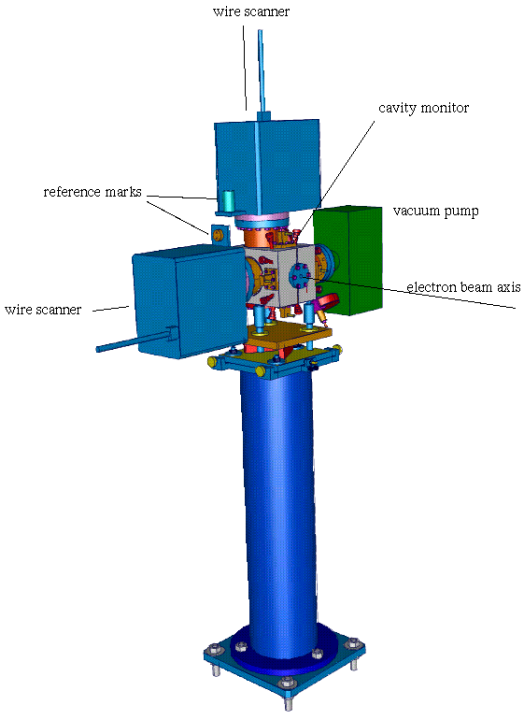

Fig. 2. Diagnostic block: Two wire scanners with reference marks are shown

2. Different Type of Monitors for the Undulator

To measure the orbit deviations due to quadrupole errors two different methods can be used.

1. the absolute beam position in respect to the undulator axis can be measured at several points of support and then be corrected. This is done by calibrated wire scanners [2, 3, 4], which allow the electron beam position to be measured in the reference frame of the undulator.

2. In a second step a beam based alignment procedure is used to reduce the offset over the entire undulator [5, 6].

2.1. Absolute Beam Position Measurement

The absolute error of the electron beam orbit with respect to the undulator axis is measured by means of several wire scanners which are located before, after and between the undulator sections. The wire scanner uses a carbon or quartz wire of 7 μm diameter, which moves through the beam. The beam profile is obtained by measuring the bremsstrahlung emitted from electrons hitting the wire as a function of the wire position [2], [3].

The same wire scanner can be used as a slow or a fast wire scanners. Slow means that for each macropulse, consisting of 800 single bunches with 1 MHz repetition rate (see table 1), only one position inside the beam pipe is measured without moving the wire.
Fast means that during one macropulse the full beam profile and position is measured. In both cases the wire scanner cannot give the beam position with only one single electron bunch.

The wire scanners define a reference axis through the entire undulator with an absolute accuracy better than 15 μm. This is achieved by calibrating the wire position in respect to the reference mark on the wire scanner front plate (see figure 2). This is done before the installation of the complete assembly. The reference mark is then used to define the position of the wire in the undulator coordinate system after the installation of the complete undulator system.
The resolution of the beam position measurement with the wire scanner is of the order of 1 μm [3].
In a second step the wire scanners can be used

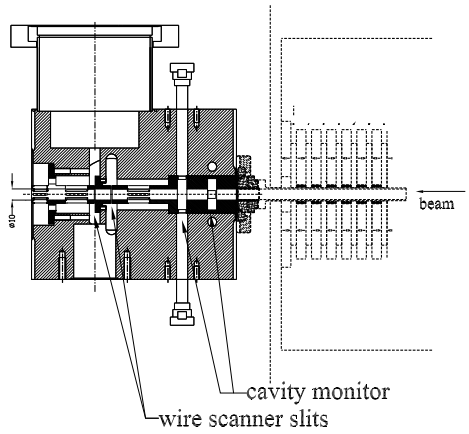

Fig. 3. Cut through the diagnostic block showing the end of an undulator section. The beam is coming from the right. On the left the slits in the beam pipe are visible which allow the wire to pass through the beam.

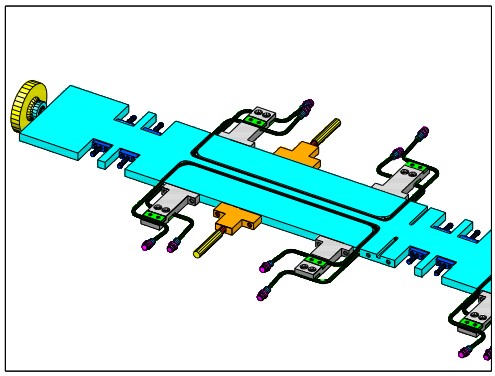

Fig. 4. Typical section of the undulator chamber [10]. Steerer windings and the 4 channels of the BPMs are visible.

to calibrate a cavity monitor [7] which is located in the same diagnostic block (see 3). The cavity monitor is a non-destructive device and allows the position of a single electron bunch to be measured. This is the reason why after calibration the cavity monitor will be the standard device for orbit measurements.
To allow this calibration both monitors are located in a so-called diagnostic block. Each diagnostic block contains a pair of wire scanners for horizontal and vertical beam profile and position measurement and a cavity monitor (figure 2). A cut through the diagnostic block is given in figure 3.

2.2. Beam Based Alignment

Figure 4 shows the undulator chamber [10] with integrated BPMs and correctors. For each quadrupole inside the undulator a corrector and BPM is integrated into the chamber. Two types of BPMs are used, both optimized for short electron bunches and both allowing a single bunch position measurement with an accuracy of 1 μm [8, 9]. This should allow the trajectory inside the undulator to be optimised to the desired rms value of less than 10 μm [5, 6].

3. Procedure to Align the Electron Beam

Different phases can be distinguished:

3.1. Startup

To get the electron beam through the undulator all BPM's can be used without any additional alignment or calibration. The accuracy due to mechanical and electrical tolerances of the monitors of a few hundred micro meters is sufficient.
To protect the undulator against radiation damage the startup will be done with only a few single bunches in the macropulse, a reduced macropulse repetion rate and a reduced charge per electon bunch (0.1 nC instead of 1 nC, see table 1). All types of monitors are able to work in this mode.

3.2. Beam position in the Absolute Reference System

The next step is to measure the electron beam position in the reference frame of the undulator with the wire scanners inside the diagnostic blocks. The electron trajectory is now fixed at 4 points with an accuracy better than 15 μm.

3.3. Beam Based Alignment

Using the BPM's and corrector coils inside the undulator sections (see 4, 5) it should be possible to achieve a straight orbit within the needed 10 μm [5, 6].

4. Measurement of Optical Mismatching

The beam optic before the undulator must be matched to the optic of the undulator to obtain a regular optic inside the undulator. Due to the

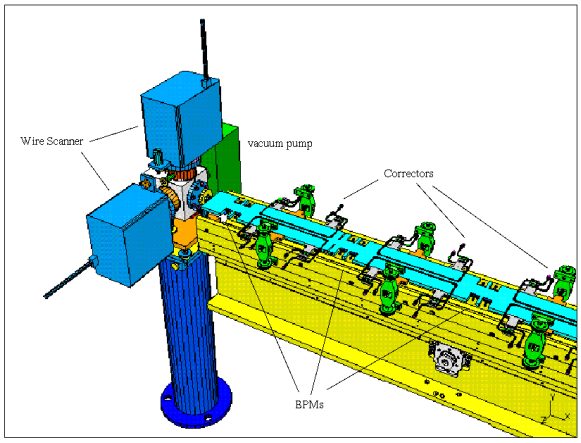

Fig. 5. Diagnostic block with part of the undulator chamber. The BPMs and correctors are visible.

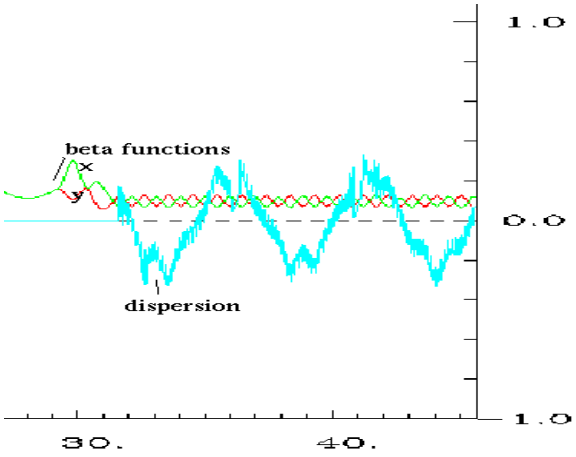

Fig. 6. The beta functions (β) and the horizontal dispersion ($D(s)$) are shown for a matched optic at a beam energy of 200 MeV. (x-axis: Longitudinal position in [m], undulator starts at 32 m.) The vertical dispersion is ≈ 0.
(y-axis: The beta function is shown as $(\sqrt{\frac{\beta}{m}} \cdot \frac{1}{10})$ and the horizontal dispersion is shown as $(\frac{-D(s)}{m} \cdot \frac{1}{10000})$.)

constant gradient of the quadrupoles the matching depends on the beam energy. Figure 6 shows a matched optic. A mismatching causes a beta beat which can be measured with help of the wire scanners. Figure 7 shows a mismatched optic.

5. Conclusion

The electron beam diagnostic will allow an easy start up of the FEL undulator. In a second step

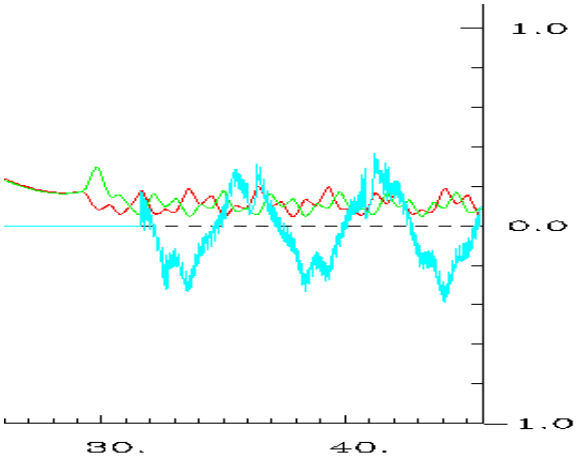

Fig. 7. The beta functions and horizontal dispersion are shown for a mismatched optic at a beam energy of 200 MeV. Same units as in figure 6 are used.

the necessary precision of the beam trajectory can be achieved by a precise measurement of the electron beam orbit in the reference frame of the undulator and with a beam based alignment procedure. The wire scanners check the correct matching of the beam optics to the undulator.

References

[1] A VUV Free Electron Laser at the TESLA Test Facility: Conceptual Design report, DESY Print TESLA-FEL 95-03, Hamburg, 1995

[2] K. Wittenburg, H. Schultz; DESY; A Proposal for using Wire Scanners at the LINAC Test Facilities; DESY-TESLA 94-15 (1994).

[3] G. Schmidt, S. Striganov, K. Wittenburg, Estimation of the TTF-FEL Wire Scanner Signal, Internal Report.

[4] With support from the Beam Instrumentation Group (BI), Cern.

[5] P. Castro; Orbit Correction by Dispersion Minimization in an Undulator with Superimposed FODO Lattice, Proc. 1998 EPAC, Stockholm

[6] K. Flöttmann, B. Faatz, E. Czuchry, J. Roßbach, Beam Based Alignment Procedure for an Undulator with Superimposed FODO Lattice, DESY Print TESLA-FEL 97-05, Hamburg 1997

[7] R. Lorenz, T. Kamps, M. Wendt, Beam Position Measurement inside the FEL Undulator at the Tesla Test Facility Linac, Proceedings of DIPAC 97, Frascati, Italy, p.73-75

[8] T. Kamps et al., *New Microwave Beam Position Monitors for the TESLA Test Facility FEL*, 8th Beam Instrumentation Workshop, SLAC, May 4 - 7, 1998

[9] M. Wendt, Coaxial line monitors, privat communication.

[10] The chamber is built in collaboration with the Experimental Facility Devision of the Advanced Photon Source (APS), Argonne.